

Reconstruction of the Altyn Tagh fault based on U-Pb geochronology: Role of back thrusts, mantle sutures, and heterogeneous crustal strength in forming the Tibetan Plateau

Eric Cowgill,¹ An Yin, and T. Mark Harrison

Department of Earth and Space Sciences and Institute of Geophysics and Planetary Physics, University of California, Los Angeles, California, USA

Wang Xiao-Feng

Institute of Geomechanics, Chinese Academy of Geological Sciences, Beijing, China

Received 7 July 2002; revised 1 January 2003; accepted 25 February 2003; published 25 July 2003.

[1] Reconstructing deformation along the northwestern margin of the Tibetan Plateau is critical for evaluating the relative importance of microplate versus continuum models of the Indo-Asian collision. Questions regarding this margin's evolution are as follows: (1) What is the total offset along the sinistral Altyn Tagh strike-slip system? (2) How has that offset been absorbed in the western Kunlun Shan? (3) Why does the N-S width of the plateau vary along strike? Ion microprobe U-Pb zircon apparent ages of 17 plutons from NW Tibet, together with regional geologic observations, define a discrete, E-W trending boundary between two tectonic belts that has been offset along the Altyn Tagh system by 475 ± 70 km. Kinematic arguments indicate that this offset cannot be the result of north directed thrusting in the western Kunlun Shan. Therefore we propose that south directed faulting in the Tianshuihai thrust belt both offset the tectonic boundary and produced the asymmetry in the plateau. Shortening appears to have been absorbed in the upper crust by thin-skinned thrusting, in the middle/lower crust by east directed ductile flow and/or subduction, and in the mantle by north dipping subduction. Factors controlling the formation of the south directed thrust system appear to be the contrast between the rigid Tarim and the weaker Songpan-Ganzi flysch belt and a mantle suture inherited from late Paleozoic subduction. The evolution of western Tibet leads to a view of continental deformation that integrates elements of the microplate model (e.g., plate-like mantle and crust-mantle decoupling) with aspects of the continuum model (weak crustal flow beneath the plateau). **INDEX TERMS:** 8102 Tectonophysics: Continental contractional orogenic belts; 8110 Tectonophysics: Continental tectonics—general (0905); 8150 Tectonophysics: Plate boundary—general (3040); 8159 Tectonophysics: Rheology—crust and lithosphere; **KEYWORDS:** Altyn Tagh fault, heterogeneous continental deformation

Citation: Cowgill, E., A. Yin, T. M. Harrison, and W. Xiao-Feng, Reconstruction of the Altyn Tagh fault based on U-Pb geochronology: Role of back thrusts, mantle sutures, and heterogeneous crustal strength in forming the Tibetan Plateau, *J. Geophys. Res.*, 108(B7), 2346, doi:10.1029/2002JB002080, 2003.

1. Introduction

[2] Although it has long been known that continental deformation is diffuse [Dewey and Sengör, 1979; Isacks *et al.*, 1968; McKenzie, 1972, 1970] a complete understanding of continental tectonics remains elusive. There are presently two end-member descriptions of continental deformation. In the first view, continents comprise mosaics of strong blocks bounded by weak faults [Kong and Bird, 1996; McKenzie, 1972, 1970; Peltzer and Tapponnier, 1988; Tapponnier and Molnar, 1976]. These blocks are either viewed as litho-

spheric scale microplates [Peltzer and Tapponnier, 1988] or blocks of mantle lithosphere that are at least partially decoupled from the overlying continental crust [Tapponnier *et al.*, 2001]. In the second view, deformation is thought to be fundamentally continuous within either a middle to lower crustal channel [Bird, 1991; Clark and Royden, 2000; McQuarrie and Chase, 2000; Royden, 1996; Shen *et al.*, 2001] or throughout the entire continental lithosphere (e.g., the thin viscous sheet models of England and Houseman [1988], England and McKenzie [1982], and Vilotte *et al.* [1982]). Although the debate over which of these two views is most appropriate is long-standing, distinguishing between them is important. If the microplate view is correct, continental deformation can be described in kinematic terms alone; whereas the continuum perspective requires understanding the dynamics of deformation.

¹Now at California Institute of Technology, Pasadena, California, USA.

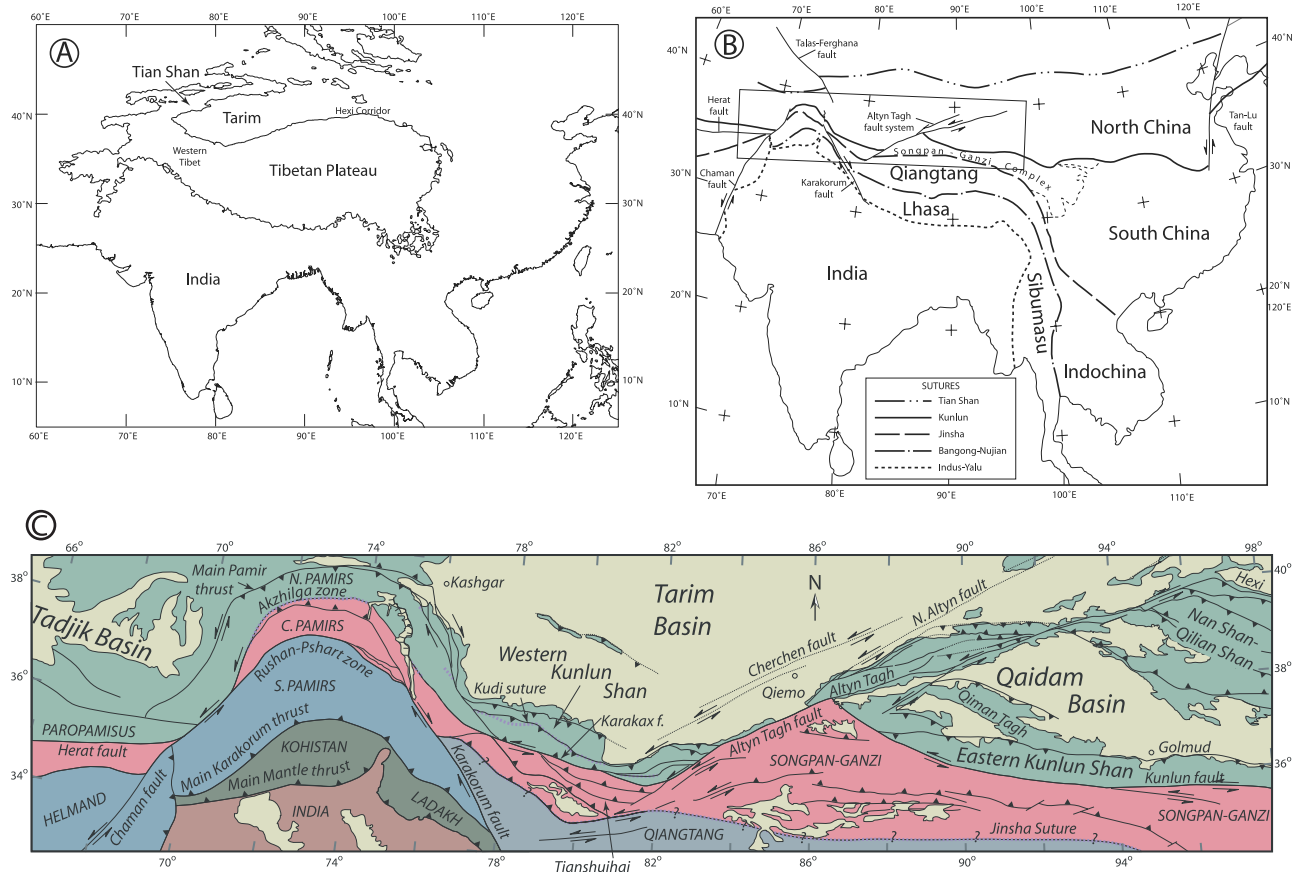


Figure 1. Overview maps of the Indo-Asian collision zone and the Tibetan Plateau. (a) Map showing the pronounced asymmetry in the north-south width of the Tibetan Plateau. At 95°E longitude the width of the Tibetan Plateau is over 3 times that at 80°E longitude. The Tibetan Plateau and Tian Shan ranges to the north are outlined by the 2000 m elevation contour. (b) Simplified tectonic map of the Tibetan Plateau showing sutures between the peri-Gondwanan fragments that were accreted to the southern margin of Eurasia during the Phanerozoic. Correlation of sutures across the Karakorum fault and the eastern Pamirs is based on the work of *Burtman and Molnar* [1993] and *Yin and Harrison* [2000], while correlations across the Chaman fault and the western Pamirs are based on the work of *Girardeau et al.* [1989] and *Burtman and Molnar* [1993]. Box outlines location of Figure 1c. (c) Tectonic map of northern Tibet. Areas shown in pink to the west of 78°E longitude may correlate with both the Qiangtang and Songpan-Ganzi belts. Base map from the work of *Liu* [1988] modified by our own observations and additional reports [*Arrowsmith and Strecker*, 1999; *Burtman and Molnar*, 1993; *Girardeau et al.*, 1989; *Hamburger et al.*, 1992; *Stöcklin*, 1989; *Strecker et al.*, 1995; *Yin and Harrison*, 2000].

[3] Asia contains the largest active continental collision on Earth and is the only continent to have been assembled during the Phanerozoic [e.g., *Sengör and Natal'in*, 1996]. As such, it provides an excellent opportunity to better understand continental deformation, and in particular, the degree to which the history of continental assembly controls subsequent deformation [e.g., *Molnar and Tapponnier*, 1981; *Yin and Harrison*, 2000; *Yin and Nie*, 1996]. One of the most striking aspects of the Indo-Asian collision is the dramatic along-strike variability in the width of the orogen (Figure 1a). A number of the peri-Gondwanan fragments that make up the Tibetan Plateau also show this westward narrowing (Figure 1b). The narrow portion of the plateau coincides with both a north directed thrust belt along the northern margin of the western Kunlun Shan and the southwestern termination of the active, left-lateral Altn Tagh strike-slip fault system (Figure 1c). According to the microplate view, this region has been narrowed by the

eastward extrusion of Tibet during simultaneous slip on the conjugate Karakorum and Altn Tagh strike-slip faults (Figures 1b and 1c) [*Molnar and Tapponnier*, 1975; *Peltzer and Tapponnier*, 1988; *Tapponnier and Molnar*, 1976]. Alternatively, in the continuum view the Tarim basin has acted as a rigid inclusion producing asymmetric deformation within the surrounding weaker lithosphere [*Clark and Royden*, 2000; *England and Houseman*, 1985; *Houseman and England*, 1996; *Vilotte et al.*, 1984].

[4] Understanding the evolution of the Altn Tagh-western Kunlun fault system is critical for distinguishing between the microplate and continuum explanations for the asymmetry of Tibet and thus for evaluating the relative significance of these two end-member views. Although the potential significance of the Altn Tagh system is clear [*Molnar and Tapponnier*, 1978, 1975; *Tapponnier and Molnar*, 1976, 1977] two critical aspects of its evolution remain poorly understood: (1) the total strike-slip offset and

(2) how this offset has been absorbed at the southwestern end of the fault system.

[5] We address these questions by measuring U-Pb zircon apparent ages to determine if batholithic belts in the western and eastern Kunlun Shan correlate (Figure 1c). These data constrain the position of a discrete tectonic boundary that has been offset along the Altyn Tagh system by 475 ± 70 km. As we demonstrate below, presently active north directed thrusts in the western Kunlun Shan cannot account for this offset. Therefore we hypothesize that slip was absorbed at the southwestern end of the Altyn Tagh fault by the Tianshuihai belt, a south directed thrust system that shortened western Tibet and produced the strong asymmetry in the north-south width of the Tibetan Plateau.

2. Tectonic Setting

[6] The Altyn Tagh fault system defines the northwestern margin of the Tibetan Plateau (Figures 1b and 1c). At its northeastern end, the fault links with thrust belts in the Nan Shan-Qilian Shan (Figure 1c) [Meyer *et al.*, 1998; Molnar and Tapponnier, 1975; Tapponnier *et al.*, 1990; Tapponnier and Molnar, 1977]. Left slip on the Altyn Tagh fault feeds into shortening within these belts, allowing Tibet to move northeast relative to Tarim [Burchfiel *et al.*, 1989; Meyer *et al.*, 1998; Yin and Nie, 1996].

[7] The kinematic picture is less clear at the southwestern end of the Altyn Tagh system, where Tarim-Tibet relative motion is thought to be absorbed in one of two ways: (1) the Tarim basement underthrusts the western Kunlun Shan along a south dipping fault system [Avouac and Peltzer, 1993; Matte *et al.*, 1996], possibly resulting in intracontinental subduction [Arnaud *et al.*, 1992; Mattauer, 1986; Matte *et al.*, 1996]; or (2) convergence is absorbed by east directed extrusion of Tibet along the conjugate Altyn Tagh and Karakorum strike-slip faults [Peltzer and Tapponnier, 1988].

[8] Previous estimates of total offset along the Altyn Tagh fault vary by an order of magnitude. Molnar and Tapponnier [1975] speculated that the Altyn Tagh range to the north of the fault has been offset ~ 400 km from the Nan Shan-Qilian Shan ranges (Figure 1c). Burchfiel and Royden [1991] extrapolated the Plio-Quaternary slip rate over the inferred duration of faulting to suggest a total offset of ~ 200 km. Similarities between Triassic strata in the western and eastern Kunlun Shan (Figure 1c) led Jiang *et al.* [1992] to conclude that the Altyn Tagh fault has offset these two belts 200–300 km. Reconstruction of shortening within the Nan Shan thrust belt (Figure 1c) led Yin and Harrison [2000] to infer at least 360 ± 50 km of left slip offset along the eastern half of the Altyn Tagh fault, similar to the 400 ± 60 km offset obtained by reconstruction of a Jurassic facies boundary [Ritts and Biffi, 2000]. Chen *et al.* [2002] used paleomagnetic data to conclude that total offset since 24 Ma is 500 ± 130 km. Pan [1984], Peltzer and Tapponnier [1988], and Pan [1996b] have correlated the western and eastern Kunlun Shan belts (Figure 1c) on the basis of their similar geology, yielding estimated offsets between 300 and 500 km. In contrast, correlations between the western Kunlun Shan and the Qilian Shan (Figure 1c) proposed by Zhang [1985], Zhu [1986] and the Chinese State Bureau of Seismology [1992] suggest that the total offset could be over 1200 km.

[9] Recent structural mapping indicates that the central Altyn Tagh fault system is a strike-slip shear zone that is ~ 100 km wide across strike [Cowgill, 2001; Cowgill *et al.*, 2000] (Figure 1c). A regional marker is needed to determine total offset due to the complexity and width of this system. Although sutures could serve this purpose [e.g., Chinese State Bureau of Seismology, 1992; Sobel and Arnaud, 1999; Yin and Nie, 1996], establishing correlations is hampered by extensive deformation of the suture belts in the western Kunlun Shan and Altyn Tagh region, and the possibility that these materials represent a complex series of back arc basins [Hsü, 1988; Hsü *et al.*, 1995; Yao and Hsü, 1992] or materials entrained within subduction-accretion complexes [Sengör, 1992; Sengör and Natal'in, 1996; Sengör and Okrogullari, 1991].

[10] An alternative approach is to use offset plutonic belts. Similarities have been noted for some time between the intrusive histories of the western and eastern Kunlun Shan [Pan, 1996a; Peltzer and Tapponnier, 1988; Yin and Nie, 1996; Zhang *et al.*, 1984], and led previous workers to suggest that this belt has been offset by the Altyn Tagh fault [Pan, 1984, 1996a; Peltzer and Tapponnier, 1988; Yin and Nie, 1996]. Batholiths in the western and eastern Kunlun Shan are thought to comprise an early to middle Paleozoic arc [Matte *et al.*, 1996; Mattern *et al.*, 1996; Pan, 1996b]. A younger (Permo-Triassic) arc is thought to have been superimposed on the southern margin of the older province during north directed subduction [Matte *et al.*, 1996; Mattern *et al.*, 1996; Pan, 1996b; Sengör, 1984]. Two issues cloud these interpretations. First, the timing of plutonism has not been well determined. Second, the spatial extent of these magmatic belts remains unclear. We present ion microprobe U-Pb zircon ages from these batholiths to establish their crystallization ages, test the proposed regional correlations, and quantify total offset along the Altyn Tagh fault system.

3. U-Pb Zircon Analyses

3.1. Methods

[11] U-Pb apparent ages were determined from 17 zircon samples using the UCLA CAMECA ims 1270 ion microprobe following procedures reported by Quidelleur *et al.* [1997]. Analyses were made using a 3–8 nA O^- primary beam focused to a spot of ~ 20 μm diameter. Secondary ionization of Pb^+ was enhanced by flooding the sample with O_2^- at a pressure of $\sim 3 \times 10^{-5}$ torr (1 torr = 133.3 N/m²). A mass resolving power of ~ 6000 was used to distinguish the ^{204}Pb peak from $^{176}Hf^{28}Si^+$, the principal molecular interference in zircon analysis [Compston *et al.*, 1984]. The $^{238}U^+$ peak was measured with a 3.5 or 5 eV offset. On average, ~ 10 zircon grains were analyzed per sample, typically with a single spot analysis per grain. Weighted mean ages of zircon standard AS3 yielded a dispersion of $<1\%$ from the canonical value of 1099.1 ± 0.5 Ma determined by thermal ionization mass spectrometry [Paces and Miller, 1993].

3.2. Results

[12] Isotope ratios and apparent ages for all samples are presented in Table 1, corrected for common Pb using the measured ^{204}Pb and the weighted mean isotopic composi-

Table 1. Ion Microprobe U-Pb Analytical Results Corrected for Common Pb

Analysis ^a	²⁰⁶ Pb/ ²³⁸ U		²⁰⁷ Pb/ ²³⁵ U		Age, ^b Ma	²⁰⁷ Pb/ ²³⁵ U I SE		²⁰⁷ Pb/ ²⁰⁶ Pb I SE		Percent ²⁰⁶ Pb/ ²³⁸ U	²⁰⁶ Pb/ ²³⁸ U I SE		²⁰⁷ Pb/ ²³⁵ U I SE		²⁰⁷ Pb*/ ²³⁵ U		²⁰⁶ Pb*/ ²³⁸ U		²⁰⁷ Pb*/ ²⁰⁶ Pb		²⁰⁷ Pb*/ ²⁰⁶ Pb I SE		CC ^d	U O/U	Th/U								
	I	SE	I	SE		I	SE	I	SE		I	SE	I	SE	I	SE	I	SE	I	SE	I	SE				I	SE						
<i>Sample 1: A196-9-13-2</i>																																	
W2 r1 g1 s1	482.9	14.70	486.3	13.1	13.1	502.1	23.8	99.8	0.078	0.002	0.614	0.021	0.057	0.001	0.948	11.8	0.20																
W2 r1 g27 s1	459.5	29.40	406.9	47.7	294.0	118.4	98.2	0.074	0.005	0.493	0.070	0.048	0.006	0.481	11.6	0.89																	
W2 r1 g41 s1	452.4	16.30	471.0	24.5	90.2	562.5	99.7	0.073	0.003	0.590	0.038	0.059	0.002	0.806	11.6	0.65																	
W2 r1 g45 s1	507.3	11.80	490.1	14.2	54.2	410.8	99.1	0.082	0.002	0.620	0.023	0.055	0.001	0.754	10.9	2.35																	
W2 r1 g47 s1	465.1	14.30	422.5	36.5	22.0	196.4	98.4	0.075	0.002	0.516	0.054	0.050	0.005	0.435	11.6	1.29																	
W2 r1 g48 s1	484.1	9.24	470.8	9.2	32.2	406.9	99.4	0.078	0.002	0.590	0.014	0.055	0.001	0.807	11.0	0.30																	
W2 r1 g5 s1	452.0	16.50	414.9	24.3	136.0	213.7	98.7	0.073	0.003	0.505	0.036	0.050	0.003	0.565	11.8	0.64																	
W2 r1 g57 s1	414.2	16.40	378.2	25.7	148.0	162.7	99.0	0.066	0.003	0.451	0.037	0.049	0.003	0.647	11.9	0.69																	
W2 r1 g60 s1	462.3	20.50	468.6	25.5	110.0	499.9	99.5	0.074	0.003	0.574	0.040	0.057	0.003	0.681	11.5	0.68																	
W2 r1 g8 s1	357.9	13.00	365.0	12.0	27.5	410.6	99.8	0.057	0.002	0.433	0.017	0.055	0.001	0.950	12.3	0.09																	
W2 r1 g7s2	389.2	25.70	408.8	26.3	76.1	521.2	97.8	0.062	0.004	0.496	0.039	0.058	0.002	0.897	10.3	0.13																	
W2 r1 g8s2	443.3	17.30	442.5	16.9	55.1	438.0	98.4	0.071	0.003	0.546	0.026	0.056	0.001	0.852	9.1	0.13																	
<i>Sample 2: 96-10-1-1b</i>																																	
W2 r3 g10 s1	486.2	14.50	480.5	14.9	44.2	453.8	99.7	0.078	0.002	0.605	0.024	0.056	0.001	0.862	11.3	0.16																	
W2 r3 g12 s1	426.9	10.20	398.6	21.6	132.0	237.2	93.8	0.068	0.002	0.481	0.032	0.051	0.003	0.507	11.6	0.42																	
W2 r3 g16 s1	484.3	11.30	475.9	10.0	22.0	435.6	99.8	0.078	0.002	0.598	0.016	0.056	0.001	0.926	11.7	0.16																	
W2 r3 g17 s1	465.6	12.60	454.2	11.9	31.9	396.8	99.4	0.075	0.002	0.564	0.018	0.055	0.001	0.900	11.8	0.47																	
W2 r3 g20 s1	495.4	14.00	488.2	11.4	17.8	454.3	99.7	0.080	0.002	0.617	0.018	0.056	0.000	0.963	12.0	1.60																	
W2 r3 g27 s1	466.4	11.00	458.0	10.6	43.4	416.3	99.7	0.075	0.002	0.570	0.016	0.055	0.001	0.746	11.7	0.54																	
W2 r3 g30 s1	462.3	12.40	449.0	10.9	22.9	381.4	99.7	0.074	0.002	0.556	0.017	0.054	0.001	0.941	11.9	0.42																	
W2 r3 g5 s1	386.0	9.86	361.2	12.0	62.6	205.0	97.8	0.062	0.002	0.427	0.017	0.050	0.001	0.731	11.9	0.34																	
W2 r3 g25s1r	499.1	6.32	484.0	6.7	26.3	413.0	99.7	0.081	0.001	0.611	0.011	0.055	0.001	0.737	9.5	0.59																	
W2 r3 g26s1c	504.3	25.60	472.4	23.1	73.4	320.2	99.7	0.081	0.001	0.592	0.036	0.053	0.002	0.849	9.0	0.90																	
W2 r3 g26s2r	455.8	7.78	443.8	13.2	66.5	382.0	98.7	0.073	0.001	0.548	0.020	0.054	0.002	0.602	9.5	0.36																	
W2 r3 g8s1	481.1	5.77	477.9	6.7	31.9	462.5	99.9	0.077	0.001	0.601	0.011	0.056	0.001	0.581	9.5	0.18																	
W2 r3 g9s1c	463.6	8.66	459.2	11.1	49.7	437.6	99.3	0.075	0.001	0.572	0.017	0.056	0.001	0.670	9.6	0.54																	
<i>Sample 3: 96-9-19-1b</i>																																	
W2 r4 g15 1	432.9	10.10	434.5	10.9	43.5	442.6	99.6	0.069	0.002	0.534	0.017	0.056	0.001	0.774	11.3	0.28																	
W2 r4 g2 s2	478.7	15.40	468.7	12.9	28.2	419.8	99.8	0.077	0.003	0.587	0.020	0.055	0.001	0.931	10.7	0.36																	
W2 r4 g3 s1	461.6	12.10	459.1	11.2	33.9	447.0	99.6	0.074	0.002	0.572	0.017	0.056	0.001	0.865	10.8	0.36																	
W2 r4 g31 s1	480.6	12.90	475.1	19.1	89.2	448.7	99.7	0.077	0.002	0.597	0.030	0.056	0.002	0.603	10.7	0.04																	
W2 r4 g25s1c	458.1	6.61	448.2	8.5	61	397.8	100	0.074	0.001	0.555	0.013	0.055	0.001	0.562	9.5	0.33																	
W2 r4 g25s2r	442.9	9.12	441.7	10.2	35.4	435.7	99.9	0.071	0.002	0.545	0.016	0.056	0.001	0.833	9.4	0.28																	
W2 r4 g29s1c	433.0	14.60	430.0	12.7	23.3	414.3	99.9	0.069	0.002	0.527	0.019	0.055	0.001	0.958	9.8	0.29																	
W2 r4 g5 1s2r	455.9	5.23	451.2	9.0	45.4	427.0	99.7	0.073	0.001	0.559	0.014	0.055	0.001	0.578	9.4	0.34																	
W2 r4 g35s1c	431.3	16.30	429.3	14.9	35.2	418.6	99.9	0.069	0.003	0.526	0.022	0.055	0.001	0.929	9.8	0.31																	
W2 r4 g39s1c	462.5	11.60	464.9	16.8	77.2	476.7	98.8	0.074	0.002	0.581	0.026	0.057	0.002	0.634	9.6	0.27																	
W2 r4 g39s2r	428.6	5.18	424.6	11.9	70.4	407.2	98.8	0.069	0.001	0.519	0.018	0.055	0.002	0.396	9.4	0.28																	
W2 r4 g4s2r	453.3	11.20	450.1	11.0	45.0	434.0	99.9	0.073	0.002	0.558	0.017	0.056	0.001	0.751	9.6	0.29																	
W2 r4 g7s1c	460.1	5.63	462.8	15.4	85.8	475.8	98.8	0.074	0.001	0.577	0.024	0.057	0.002	0.362	9.4	0.38																	
W2 r4 g7s2r	468.5	7.64	464.4	9.8	40.1	444.2	99.7	0.075	0.001	0.580	0.015	0.056	0.001	0.732	9.3	0.43																	
<i>Sample 4: 96-8-22-4b</i>																																	
W2 r6 g35 s1	492.6	24.90	488.8	23.3	68.7	470.8	99.9	0.079	0.004	0.618	0.037	0.056	0.002	0.856	10.4	0.43																	
W2 r6 g47 s1	472.5	24.70	481.9	25.1	83.3	526.9	99.8	0.076	0.004	0.607	0.040	0.058	0.002	0.814	10.4	0.35																	
W2 r6 g50 s1	508.3	33.80	494.1	29.6	72.9	428.5	99.8	0.082	0.006	0.627	0.047	0.055	0.002	0.902	10.2	0.52																	
W2 r6 g8 s1	447.2	34.50	439.4	34.9																													

Table 1. (continued)

Analysis ^a	²⁰⁶ Pb/ ²³⁸ U		²⁰⁷ Pb/ ²³⁵ U		Age, ^b Ma		Percent ²⁰⁶ Pb/ ²³⁸ U		²⁰⁶ Pb*/ ²³⁸ U		²⁰⁷ Pb*/ ²³⁵ U		²⁰⁷ Pb*/ ²⁰⁶ Pb*		CC ^d		U O/U		Th/U		
	1 SE	1 SE	1 SE	1 SE	1 SE	1 SE	1 SE	1 SE	1 SE	1 SE	1 SE	1 SE	1 SE	1 SE	1 SE	1 SE	1 SE	1 SE	1 SE	1 SE	
A2 r4g23 s1	425.7	7.60	430.7	9.1	457.8	9.8	99.8	0.068	0.001	0.528	0.014	0.056	0.841	8.3	0.841	8.3	0.23				
A2 r4g36 s1	426.4	7.32	420.3	9.4	386.8	98.1	98.1	0.068	0.001	0.513	0.014	0.054	0.624	8.6	0.624	8.6	0.73				
Sample 9: AY94-9-12-3																					
A2 r6g10 s1	454.3	7.49	467.9	48.3	535.7	89.0	89.0	0.073	0.001	0.585	0.075	0.058	0.285	8.3	0.285	8.3	0.31				
A2 r6g3 s1	474.0	5.59	479.0	5.1	502.8	99.7	99.7	0.076	0.001	0.603	0.008	0.057	0.882	8.4	0.882	8.4	0.25				
A2 r6g43 s1	545.3	12.90	598.3	56.8	804.6	77.0	77.0	0.088	0.002	0.803	0.101	0.066	0.414	8.6	0.414	8.6	1.24				
A2 r6g53 s1	488.9	5.38	490.1	8.2	495.8	99.6	99.6	0.079	0.001	0.620	0.013	0.057	0.607	8.4	0.607	8.4	0.51				
A2 r6g53 s2	708.8	12.60	692.1	46.7	638.3	76.4	76.4	0.116	0.002	0.977	0.091	0.061	0.409	8.4	0.409	8.4	0.19				
A2 r6g54 s1	478.5	5.37	480.8	5.8	491.9	100	100	0.077	0.001	0.606	0.009	0.057	0.717	8.2	0.717	8.2	0.42				
A2 r6g67 s1	467.6	6.42	471.2	6.3	488.9	99.1	99.1	0.075	0.001	0.591	0.010	0.057	0.851	8.6	0.851	8.6	0.21				
A2 r6g72 s1	525.2	4.62	515.8	17.4	474.5	98.2	98.2	0.085	0.001	0.662	0.028	0.057	0.366	8.2	0.366	8.2	0.29				
Sample 10: AY6-8-99-1																					
A3 r4g11s1	437.7	6.53	446.0	7.4	488.8	100	100	0.070	0.001	0.552	0.011	0.057	0.635	9.5	0.635	9.5	0.52				
A3 r4g12s1	450.7	5.98	460.0	12.8	506.9	98.1	98.1	0.072	0.001	0.573	0.020	0.057	0.496	9.3	0.496	9.3	1.19				
A3 r4g13s1	535.2	9.13	556.0	12.1	641.8	100	100	0.087	0.002	0.729	0.021	0.061	0.701	9.4	0.701	9.4	0.09				
A3 r4g6s1	429.9	9.03	420.3	33.3	367.9	96.8	96.8	0.069	0.002	0.513	0.050	0.054	0.506	9.5	0.506	9.5	0.52				
A3 r4g6s2	443.9	12.00	456.3	19.7	519.3	89.4	89.4	0.071	0.002	0.567	0.030	0.058	0.668	9.1	0.668	9.1	0.57				
A3 r4g7s1	408.1	6.55	418.5	7.3	476.4	100	100	0.065	0.001	0.510	0.011	0.057	0.783	9.6	0.783	9.6	0.59				
A3 r4g8s1	472.0	6.00	468.2	6.9	449.9	99.7	99.7	0.076	0.001	0.586	0.011	0.056	0.784	9.5	0.784	9.5	0.21				
A3 r4g9s1	428.2	5.83	429.4	6.3	435.9	99.9	99.9	0.069	0.001	0.526	0.010	0.056	0.829	9.2	0.829	9.2	0.07				
Sample 11: AY6-5-99-2b																					
A3 r2g10 s1	387.8	10.60	412.5	16.6	553.2	99.5	99.5	0.062	0.002	0.501	0.025	0.059	0.526	8.1	0.526	8.1	0.44				
A3 r2g24 s1	413.9	5.61	429.0	10.6	510.7	98.4	98.4	0.066	0.001	0.526	0.016	0.058	0.469	8.3	0.469	8.3	0.46				
A3 r2g29 s1	379.1	3.35	384.7	4.3	418.2	99.9	99.9	0.061	0.001	0.461	0.006	0.055	0.463	8.3	0.463	8.3	0.62				
A3 r2g6 s1	386.7	4.13	406.6	11.3	521.0	99.8	99.8	0.062	0.001	0.493	0.017	0.058	0.396	8.4	0.396	8.4	0.62				
A3 r2g7 s1	408.2	13.30	410.9	18.6	426.4	99.8	99.8	0.065	0.002	0.499	0.027	0.055	0.666	8.0	0.666	8.0	0.47				
Sample 12: AY98-8-24-3																					
A3 r6g1s1	462.4	7.67	458.6	7.1	439.7	100	100	0.074	0.001	0.571	0.011	0.056	0.791	9.0	0.791	9.0	0.38				
A3 r6g1s2	441.8	6.68	438.4	7.4	420.2	99.7	99.7	0.071	0.001	0.540	0.011	0.055	0.449	9.2	0.449	9.2	0.31				
A3 r6g2s1	409.8	5.64	411.4	6.4	420.1	25.5	100	0.066	0.001	0.500	0.010	0.055	0.801	9.6	0.801	9.6	0.42				
A3 r6g3s1	461.9	6.97	459.8	6.7	449.2	25.2	100	0.074	0.001	0.573	0.010	0.056	0.786	9.1	0.786	9.1	0.45				
A3 r6g4s1	448.7	7.09	447.6	6.9	442.0	27.5	100	0.072	0.001	0.554	0.011	0.056	0.764	9.1	0.764	9.1	0.37				
A3 r6g5s1	433.7	5.52	439.5	6.1	470.4	99.9	99.9	0.070	0.001	0.542	0.009	0.056	0.742	9.5	0.742	9.5	0.45				
A3 r6g5s2	460.9	5.86	461.0	7.6	461.7	99.6	99.6	0.074	0.001	0.575	0.012	0.056	0.679	9.4	0.679	9.4	0.33				
A3 r6g5s3	454.2	7.89	459.4	8.9	486.0	100	100	0.073	0.001	0.572	0.014	0.057	0.812	8.8	0.812	8.8	0.44				
Sample 13: AY5-18-99-7 ^e																					
N1 r1g14s1	454.7	7.80	450.4	12.4	428.4	99.9	99.9	0.073	0.001	0.558	0.019	0.055	0.654	10.0	0.654	10.0	0.92				
N1 r1g14s2r	464.5	11.70	456.7	14.3	417.5	49.5	99.9	0.075	0.002	0.568	0.022	0.055	0.839	9.5	0.839	9.5	0.89				
N1 r1g17s1	426.9	8.9	441.2	11.2	516.7	100	100	0.069	0.002	0.544	0.017	0.058	0.798	10.5	0.798	10.5	0.56				
N1 r1g32s2c	510.5	8.86	507.6	7.0	494.5	100	100	0.082	0.001	0.649	0.011	0.057	0.820	10.9	0.820	10.9	1.61				
Sample 14: AY5-20-99-4 ^f																					
N1 r4g2s1c	538.5	10.9	992.4	58.3	2202	99.9	99.9	0.087	0.002	1.66	0.153	0.138	0.671	9.2	0.671	9.2	0.58				

Table 2. Comparison of Ages Calculated Using Different Common Pb Compositions for Sample 9: AY94-9-12-3 for 24 August 1999 Analyses

Analysis	$^{206}\text{Pb}^*/^{238}\text{U}$ Age, ^a	$^{206}\text{Pb}^*/^{238}\text{U}$ Age, ^b	$^{206}\text{Pb}^*/^{238}\text{U}$ Age, ^c	$^{206}\text{Pb}^*/^{238}\text{U}$ Age, ^d	Percent $^{206}\text{Pb}^*$ ^e	Difference (LA-0SK), %	Difference (LA-450 Ma), %	Difference (LA-None), %
	Ma (LaPb)	Ma (0 SK)	Ma (450 SK)	Ma (None)				
ATz2_r6g10_s1	454.3	454.8	456.9	508.0	89.0	0.1	0.6	10.6
ATz2_r6g3_s1	474.0	474.1	474.1	475.3	99.7	0.0	0.0	0.3
ATz2_r6g43_s1	545.3	547.0	552.8	699.7	77.0	0.3	1.4	22.1
ATz2_r6g53_s1	488.9	488.9	489.0	490.9	99.6	0.0	0.0	0.4
ATz2_r6g53_s2	708.8	711.1	718.8	912.6	76.4	0.3	1.4	22.3
ATz2_r6g54_s1	478.5	478.5	478.5	478.4	100.0	0.0	0.0	0.0
ATz2_r6g67_s1	467.6	467.6	467.8	471.5	99.1	0.0	0.0	0.8
ATz2_r6g72_s1	525.2	525.3	525.7	534.3	98.2	0.0	0.1	1.7
Average					92.4	0.1	0.4	7.3

^aCorrected using modern Los Angeles environmental Pb: $^{206}\text{Pb}/^{204}\text{Pb}$, 18.911; $^{207}\text{Pb}/^{204}\text{Pb}$, 15.70; $^{208}\text{Pb}/^{204}\text{Pb}$, 38.526.

^bCorrected using zero-age Stacey-Kramers model Pb: $^{206}\text{Pb}/^{204}\text{Pb}$, 18.703; $^{207}\text{Pb}/^{204}\text{Pb}$, 15.529; $^{208}\text{Pb}/^{204}\text{Pb}$, 37.859.

^cCorrected using 450 Ma Stacey-Kramers model Pb: $^{206}\text{Pb}/^{204}\text{Pb}$, 17.99; $^{207}\text{Pb}/^{204}\text{Pb}$, 15.589; $^{208}\text{Pb}/^{204}\text{Pb}$, 37.116.

^dUncorrected for common Pb.

^ePercent radiogenic ^{206}Pb .

tion of modern aerosol lead in the Los Angeles basin [Sañudo-Wilhelmy and Flegal, 1994] (see Table 1). This composition was chosen based on the assumption that a significant fraction of the common Pb in the samples results from surface contamination introduced during sample preparation. To evaluate this assumption, we have also corrected the Pb/U ratios from the least radiogenic sample (9: AY94-9-12-3) using compositions for 0 and 450 Ma terrestrial Pb as calculated from a model of terrestrial Pb evolution [Stacey and Kramers, 1975]. As Table 2 indicates, $^{206}\text{Pb}^*/^{238}\text{U}$ apparent ages calculated using the three common Pb compositions differ by less than 1%. Over 88% of the grains analyzed in the present study contain >95% radiogenic ^{206}Pb ($^{206}\text{Pb}^*$) and are thus relatively insensitive to uncertainties in the common Pb correction. Application of the ^{204}Pb correction (aerosol composition) to sample 14 and one set of analyses of grains from sample 13 overcorrects ^{207}Pb , resulting in reversely discordant U-Pb ages. For these samples, grains with $\text{Th}/\text{U} \leq 0.5$ were corrected assuming concordancy between the U-Pb and Th-Pb systems. Grains with $\text{Th}/\text{U} > 0.5$ were corrected using ^{204}Pb .

[13] Common Pb-corrected analyses typically define a cluster of concordant ages which span 50–70 Myr (Table 1). The distribution of $^{206}\text{Pb}^*/^{238}\text{U}$ ages is shown in Figure 2 as histograms and cumulative probability plots. Six of the samples (2, 8, 9, 10, 13, and 14) contain older and/or younger analyses which are also concordant, but which were excluded from calculations of the weighted mean on the basis of the following criteria. All older analyses with peaks in the cumulative probability curve which are distinct from the maximum are interpreted as inherited zircons. Although samples 4, 7, and 11 show asymmetric $^{206}\text{Pb}^*/^{238}\text{U}$ age distributions with old tails (Figure 2), possibly reflecting either protracted crystallization resulting from magmatic recharge or recycling of zircon from earlier intrusions, these analyses are included in the weighted mean age calculation. Evaluating the significance of the younger grains is more problematic. On average, the young grains in samples 2, 8, and 14 are 4, 14, and 46%, respectively, less radiogenic in ^{206}Pb than the average of all other analyses from the same sample (Table 1). Because these young ages may result from either problems with the common Pb correction or analysis of grains which were more susceptible to younger Pb loss, these analyses were

excluded from the calculation of the weighted mean. Because sample 13 is penetratively foliated, the anomalously young age from this sample was excluded due to the possibility that it reflects Pb loss during a younger metamorphic event. Excluded analyses are indicated in Table 3.

[14] Even when these outlying ages are not included in the weighted mean, mean square weighted deviation (MSWD) values are higher than is expected for single age populations, suggesting that either the assigned analytical errors are too small or the plutons contain multiple age populations. True variability of the single grain ages could be the result of entrainment of restitic zircons during melting in the source area, incorporation of xenocrystic zircon during emplacement, protracted crystallization due to slow cooling or pulsed intrusion, or variable amounts of Pb loss subsequent to crystallization. It must be emphasized that the goal of this study is to characterize the spatial and temporal distribution of magmatism in the western Kunlun Shan, Altyn Tagh, and Nan Shan areas, rather than to resolve detailed crystallization histories. It is clear from the data presented here that northern Tibet is characterized by regionally extensive early to middle Paleozoic magmatism.

3.3. Spatial Patterns in Ages

[15] U-Pb zircon and Rb-Sr ages from northwestern Tibet are compiled in Figure 3 and show two age populations: an older suite that ranges from early to middle Paleozoic (518–384 Ma) and a younger suite that ranges from late Paleozoic to early Mesozoic (290–180 Ma). In the following section, we separate samples in the western Kunlun Shan (i.e., between 76°E and 84°E longitude) from those in the eastern Kunlun Shan, Altyn Tagh, and Nan Shan ranges (i.e., east of 84°E). We refer to these as the western and eastern areas, respectively. Both areas contain the two age populations.

[16] In the western area, the older suite ranges from Early Ordovician (478 ± 9 Ma, sample 2, 1 standard deviation) to Middle Devonian (384 ± 2 Ma, sample E) (timescale from the work of Haq and Van Eysinga [1998]). By contrast, in the eastern region, the older suite ranges from Middle Cambrian (518 ± 13 Ma, sample 7) to Middle Devonian (389 ± 5 Ma, sample 11). Despite these broad ranges, in both areas the older suite shows a pronounced

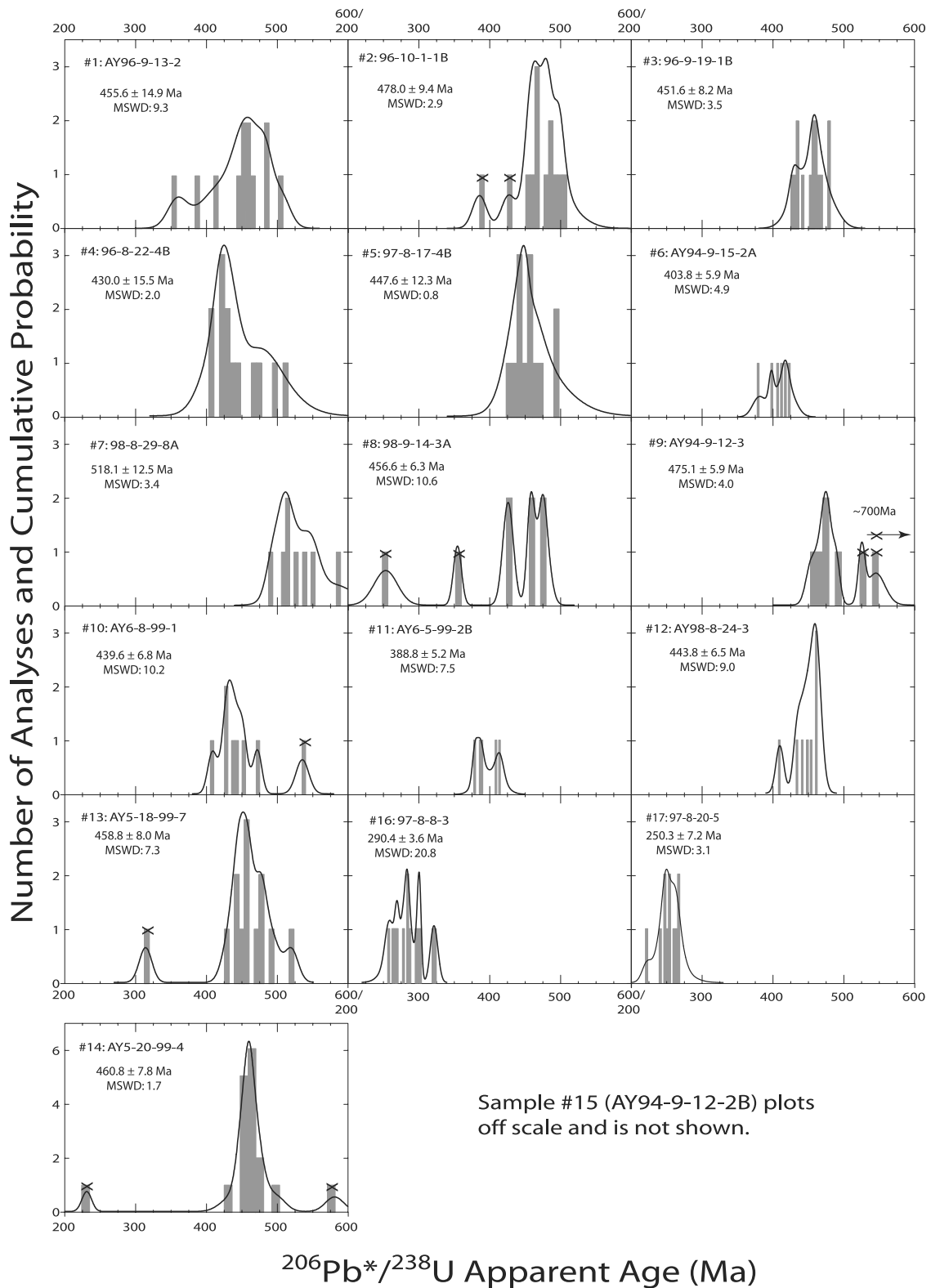


Figure 2. Cumulative probability plots of zircon $^{206}\text{Pb}^*/^{238}\text{U}$ ages with weighted mean (± 1 standard deviation) and MSWD corresponding to the main peak or group of peaks in the cumulative probability curves. Crossed out peaks were not included in calculation of weighted mean as is discussed in text. See Tables 1 and 3 for analytical results and excluded peaks, respectively.

Table 3. Weighted Mean U-Pb Apparent Ages^a

Sample: Field	Location	Latitude °N	Longitude °E	²⁰⁶ Pb*/ ²³⁸ U				²⁰⁷ Pb*/ ²³⁵ U				²⁰⁷ Pb*/ ²⁰⁶ Pb*				Removed Analyses	
				Age, Ma	SE	SD	MSWD	Age, Ma	SE	SD	MSWD	Age, Ma	SE	SD	MSWD		N ^b
1: AY96-9-13-2	Kusilaf	37.975	76.296	455.6	4.3	14.9	9.3	446.1	4.9	16.9	7.8	445.5	13.8	47.9	1.9	12/12	
2: 96-10-1-1b	Abalek	36.877	78.438	478.0	2.8	9.4	2.9	471.0	3.1	10.1	2.1	425.7	9.0	29.8	1.2	11/13	g12s1, c, g5s1 ^c
3: 96-9-19-1b	Qira	36.375	80.320	451.6	2.2	8.2	3.5	449.0	3.1	11.5	1.5	427.6	10.6	39.8	0.2	14/14	
4: 96-8-22-4b	Pulu	36.140	81.453	430.0	4.3	15.5	2.0	427.1	6.1	22.1	2.8	423.2	26.4	95.1	1.3	13/13	
5: 97-8-17-4b	Tatulekisu	37.986	86.319	447.6	3.4	12.3	0.8	434.0	11.2	40.4	0.9	393.9	64.0	230.7	0.3	13/13	
6: AY94-9-15-2A	east of Tula	37.67	87.41	403.8	2.4	5.9	4.9	414.4	3.6	8.9	1.2	412.0	17.9	43.8	2.1	6/6	
7: 98-8-29-8a	north of Gasi	38.226	88.768	518.1	4.4	12.5	3.4	523.7	5.4	15.4	2.5	558.9	18.5	52.3	3.7	8/8	
8: 98-9-14-3a	east of Gasi	38.177	89.032	456.6	2.6	6.3	10.6	458.0	3.4	8.2	7.7	462.0	12.6	30.8	1.0	6/8	g14s1, c, g15s1 ^c
9: AY94-9-12-3	Ruoqiang Hwy	38.68	89.26	475.1	2.6	5.9	4.0	479.2	3.0	6.8	0.9	496.9	9.7	21.8	0.1	5/8	g43s1, d, g53s2, d, g72s1 ^d
10: AY6-8-99-1	south of Bashikaogong	38.999	90.400	439.6	2.6	6.8	10.2	442.0	3.3	8.7	5.3	459.0	13.1	34.6	0.6	7/8	g13s1 ^d
11: AY6-5-99-2B	south of Lapeiquan	38.862	91.645	388.8	2.3	5.2	7.5	394.2	3.6	8.0	4.7	450.4	22.1	49.3	1.2	5/5	
12: AY98-8-24-3	south of Ananba	39.02	92.85	443.8	2.3	6.5	9.0	445.2	2.5	7.0	6.4	449.1	10.1	28.5	0.6	8/8	
13: AY5-18-99-7	Dang He Nan Shan	39.068	95.609	458.8	2.3	8.0	7.3	475.3	4.5	15.5	4.2	468.2	18.0	62.2	0.9	12/13	g1s1 ^e
14: AY5-20-99-4	Yema Nan Shan	39.179	95.808	460.8	2.0	7.8	1.7	473.4	4.5	17.4	1.0	537.3	22.0	85.0	1.3	15/17	g7s2r, c, g21s1c ^d
15: AY94-9-12-2b	Ruoqiang Hwy	38.62	89.29	968.9	5.8	17.3	3.0	959.4	4.6	13.8	2.2	932.5	8.7	26.2	1.3	9/9	
16: 97-8-8-3	Chumbulaka	37.577	86.040	290.4	1.0	3.6	20.8	276.6	2.0	7.2	61.1	219.2	16.1	58.0	1.1	13/13	
17: 97-8-20-5	Kulamulak	37.367	85.756	250.3	2.2	7.2	3.1	215.5	16.9	56.1	1.1	412.2	221.8	735.7	0.2	11/11	

^aReported errors are ±1 standard error (SE) and ±1 standard deviation (SD) on the weighted mean.^bNumber of analyses used to calculate weighted mean/number of analyses made.^cGrains with low %²⁰⁶Pb*, relative to others in sample.^dInherited grains.

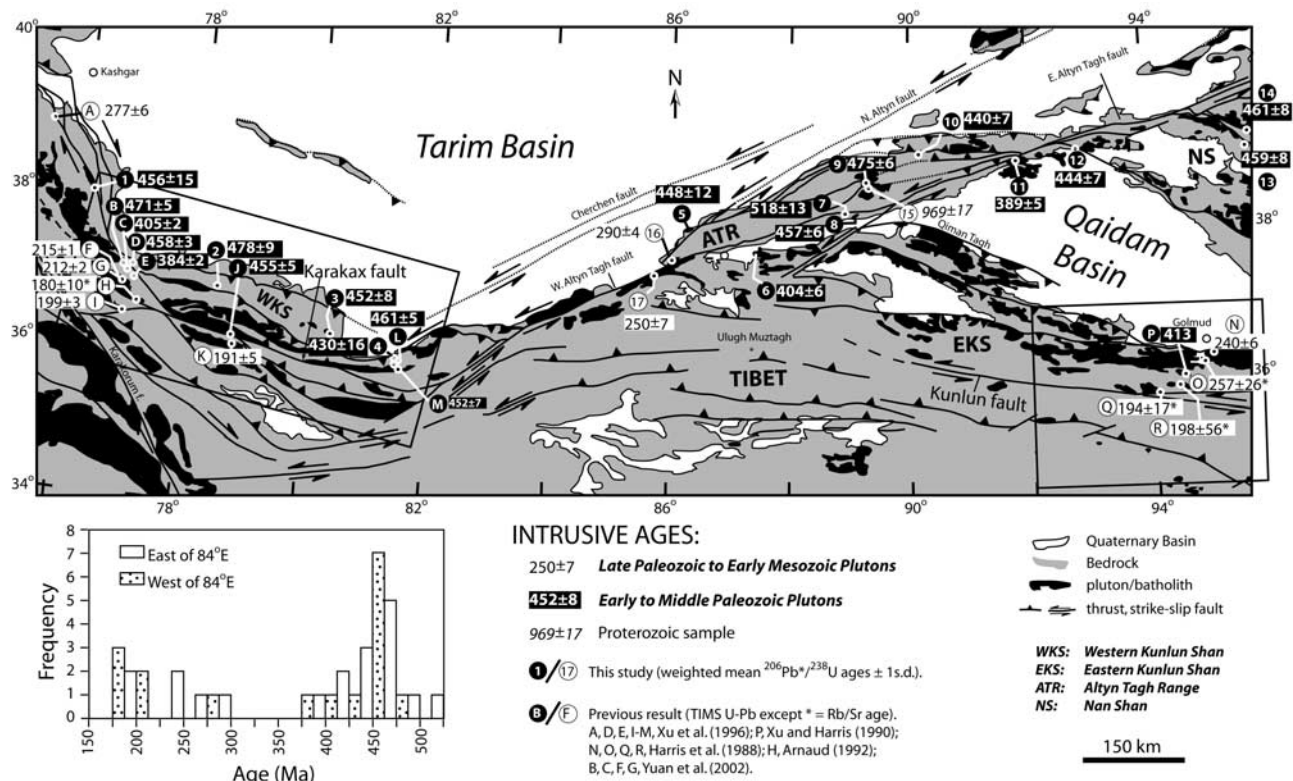


Figure 3. Map of northern Tibet showing crystallization ages compiled from this study and previous reports. Two age populations are present with an older suite shown in black boxes and a younger suite shown in white boxes. This bimodal distribution of ages is evident on the inset histogram. On the map the older suite of ages is restricted to regions north of the Karakax and Kunlun faults, whereas the younger suite is present both north and south of these markers. Results from the present study are labeled numerically and reflect weighted mean $^{206}\text{Pb}^*/^{238}\text{U}$ ion-microprobe zircon ages. Previously published ages are labeled alphabetically and represent Concordia intercept ages from multigrain aliquots analyzed by thermal ionization mass spectrometry, except for Rb-Sr ages that are denoted with an asterisk. Sources of previously published data are shown in the legend. Boxes outline the location of regional geologic maps shown in Figure 4.

concentration of Early to Late Ordovician ages (i.e., 450–475 Ma) (Figure 3).

[17] The younger population of samples spans an age range that is similar to the older suite. Samples A (277 ± 6 Ma) and H (180 ± 10 Ma) from the western area and samples 16 (290 ± 4 Ma) and Q (194 ± 17 Ma) from the eastern region indicate that the younger suite ranges from Early Permian to Early Jurassic. In the western area the younger suite shows a concentration of Early Jurassic ages between 180 and 215 Ma, whereas the eastern area has both an Early Jurassic concentration and a Late Permian to Middle Triassic peak.

[18] Although the temporal distributions of the two age populations are similar in both the western and eastern areas, the populations show important spatial variations from north to south. Figure 3 shows that samples from the older suite are restricted to areas north of the Karakax and Kunlun faults. The older plutons are widely distributed in these northern areas and show no systematic north-south variations in age, although such variations may be obscured by younger deformation or incomplete sampling. The younger suite of plutons is present both north and south of the Karakax and Kunlun faults. Thus in both the western and eastern

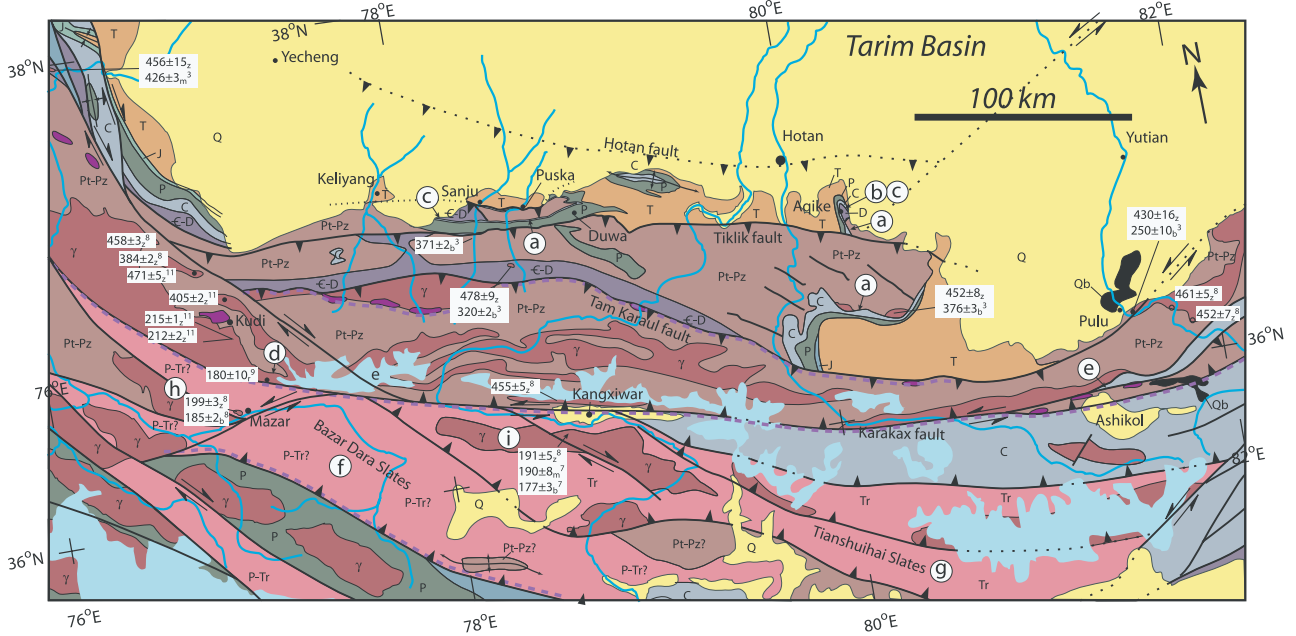
regions, a mixed distribution of young and old plutons characterizes areas in the north while only the younger phase of plutonism is present to the south.

4. Interpretation

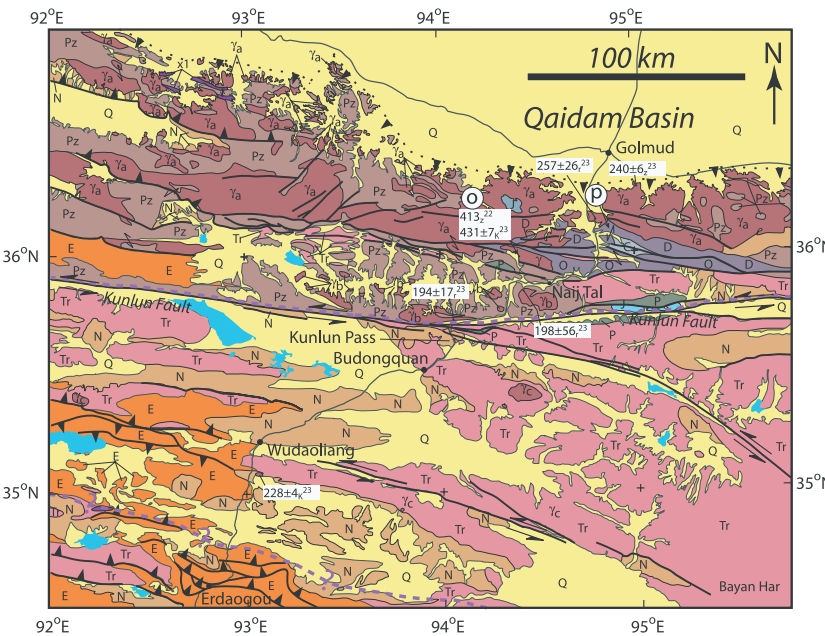
4.1. Significance of Age Pattern

[19] The pattern of plutonic ages shown in Figure 3 provides the first radiometric dates confirming earlier suggestions that a matching pair of plutonic belts is present in both the western and eastern Kunlun Shan [Pan, 1996a; Peltzer and Tapponnier, 1988; Yin and Nie, 1996; Zhang et al., 1984] and supports the interpretation that these belts have been offset along the Altyn Tagh fault system [Pan, 1984, 1996a; Peltzer and Tapponnier, 1988; Yin and Nie, 1996]. The first magmatic belt is defined by the older suite of plutons in Figure 3. It is unclear if this broad magmatic belt represents a single arc [e.g., Matte et al., 1996; Pan, 1996a], a series of island arcs [e.g., Hsü et al., 1995; Yao and Hsü, 1992], or a southward younging subduction-accretion complex [e.g., Sengör and Natal'in, 1996; Sengör and Okurogullari, 1991]. In spite of this ambiguity, Figure 3 clearly indicates that plutons of this

WESTERN KUNLUN SHAN:



EASTERN KUNLUN SHAN:



LEGEND:

(a) Locality cited in table

240±6,²³ Isotopic age determination. Superscript indicates reference (excluding values reported here). Subscript indicates method:
 z = ²⁰⁶Pb/²³⁸U zircon age
 b = ⁴⁰Ar/³⁹Ar biotite total gas or "plateau" age
 m = ⁴⁰Ar/³⁹Ar muscovite total gas or "plateau" age
 r = Rb/Sr whole-rock isochron age
 K = biotite K-Ar age

Left-lateral strike-slip fault
 Thrust/Reverse fault (barbs on upper plate)
 Fault (kinematics unknown)
 Known/Inferred Suture
 Ophiolite or ultramafic body

Granitoids: unassigned; a, mid-Paleozoic or Permian-Triassic; b, early Jurassic; c, late Triassic-early(?) Jurassic.

Quaternary: Q, undifferentiated; Qb, basalt

Tertiary: E, Paleogene; N, Neogene; T, undifferentiated

Jurassic: Rare. Generally terrestrial.

Triassic: flyschoid units.

Carboniferous, Permian.

Cambrian to Devonian, Ordovician, Devonian.

Basement: Proterozoic-Paleozoic units or undifferentiated early to mid-Paleozoic rocks.

Figure 4a. Simplified geologic maps of the western and eastern Kunlun Shan with selected geochronologic and thermochronologic data. See Figure 3 for locations of maps. Western Kunlun map compiled from Liu [1988], Xinjiang Bureau of Geology and Mineral Resources [1993], and our own observations; eastern Kunlun Shan map modified from Kidd *et al.* [1988] (with permission from The Royal Society and W.S.F. Kidd).

belt are restricted to regions north of the Karakax and Kunlun faults.

[20] The second belt is defined by the younger suite of plutons in Figure 3 and represents a Late Permian to Early Jurassic magmatic arc. This younger belt was locally superimposed upon the southern margin of the older belt, consistent with the interpretation that the younger belt formed during north directed subduction of the Paleotethys

oceanic lithosphere [Matte *et al.*, 1996; Mattern *et al.*, 1996; Pan, 1996b; Sengör, 1984].

4.2. The Offset Marker

[21] Combining the timing of plutonism (Figure 3) with thermochronologic and regional geologic data (Figure 4) indicates that the matching plutonic belts coincide with a pair of tectonic provinces (Figure 5). As we show, recog-

	WESTERN KUNLUN (bracketed letters refer to localities on upper map)	EASTERN KUNLUN (bracketed letters refer to localities on lower map)
NORTHERN TECTONIC BELT	<p>Early-Mid Paleozoic Deformation, Metamorphism, Magmatism</p> <p>*Regional mid-Paleozoic unconformity caps: (a) Mitaz schist: metapelite with 330-370 Ma biotite ⁴⁰Ar/³⁹Ar ages [3]. Protolith is late Proterozoic to early Paleozoic flysch [1,2] ? (b) Devonian or Carboniferous terrestrial clastic rocks that are overturned and faulted against Mitaz schist [3]. (c) Tilted Upper Devonian [4]. *Kunlun batholith [5,6] intrudes biotite schist, migmatitic paragneisses [7] and metavolcanic rocks [8]. See map for ages. *Mid-Paleozoic ⁴⁰Ar/³⁹Ar ages (cooling due to unroofing?) [3, 7, 9].</p>	<p>*post-Ordovician, pre-Upper Devonian deformation and metamorphism with development of highly-strained stretch pebble conglomerates, sheath folds, and well-developed cleavage [20]. *Silurian strata appear to be missing [21]. *Wanbaogou pluton (o) has 413 Ma (no error reported) U-Pb zircon age [22 cited in 8] and 431±7 Ma biotite K-Ar age [23]. *late Devonian(?) volcanics and volcanoclastic strata (p) [21].</p>
	<p>Mid-Late Paleozoic stratigraphy</p> <p>*Regionally extensive Upper Carboniferous shelf carbonates and Lower Permian clastic rocks unconformably overlie deformed lower Paleozoic strata and crystalline basement (a,b,c) [3, 5, 10]. *N-directed paleocurrents in Permian clastics [3].</p>	<p>*Metamorphic units are unconformably overlain by unmetamorphosed Devonian terrestrial strata with a basal conglomerate [21]. *NW-directed paleocurrents in Lower Carboniferous strata [24]. *Terrestrial strata overlain by Carboniferous(?) marine rocks [21,24]. *Triassic terrestrial strata locally unconformably overly Ordovician strata [21].</p>
	<p>Magmatic gap</p> <p>*No crystallization ages between 384 Ma and 277 Ma yet reported.</p>	<p>*No crystallization ages between 389 Ma and 290 Ma yet reported.</p>
	<p>Late Paleozoic Magmatism</p> <p>*See map for ages. *(d) Red porphyries with an Rb/Sr whole rock isochron age of 180±10 Ma [9].</p>	<p>*Syntectonic, calc-alkaline granitic pluton with U-Pb zircon age of 240±6 Ma intrudes foliated granodiorite [23].</p>
BOUNDARY	<p>Active, left-lateral fault</p> <p>*Karakax fault system [7, 12, 13].</p>	<p>*Kunlun fault [25, 26, 27].</p>
	<p>Contrast in metamorphic grade</p> <p>*North of the boundary: migmatites and granitic batholith of the Kunlun Shan. South of the boundary: poorly-dated, deformed slates intruded by Jurassic granitoids [5, 7, 14].</p>	<p>*North of the boundary: garnet-bearing schist. South of the boundary: lower grade metasedimentary rocks [24].</p>
	<p>Suture</p> <p>*Maqi Suture: (e) Serpentinized harzburgite, dunite, and pillow basalts occur in the Karakax fault zone [15]. *Karakax fault correlated with Anyemaqen suture [16, 17, 18] .</p>	<p>*Kunlun fault coincides with Anyemaqin suture [20, 18]. *As evidence of a suture, [20] cites: ophiolites north of Ulugh Muztagh [28], the Anyemaqen ophiolite belt (see [20] for location), and separation of North and South Cathaysian faunas [30]. *Suture marked by glaucophane schist and mélangé with exotic Permian blocks in a matrix of Permian and Triassic flysch [20, 15].</p>
SOUTHERN TECTONIC BELT	<p>Slate Belts</p> <p>Bazar Dara (f): *mélangé of exotic blocks in a pervasively sheared, schistose matrix [19]. *Poorly known protolith age. Former assignment of Silurian [5] is based on fossils from an exotic limestone slab within the mélangé and is thus unfounded [19] .</p> <p>Tianshuihai (g): *Gradational with Bazar Dara [7]. Thought to be Triassic [5]. *Contains exotic blocks of Carboniferous, Permian and Triassic carbonates in a matrix of hemipelagic sediments [19]. *Generally lower grade than Bazar Dara [7, 19].</p>	<p>The Bayan Har Group: *Poorly dated (possibly Triassic), deformed, low-grade slates [24]. *monotonous sandstones, shales, and turbidites [21].</p>
	<p>Top-to-south deformation</p> <p>*Bazar Dara is folded with north-dipping cleavage [7]. *Tianshuihai is tightly folded by south-vergent structures [7].</p>	<p>*Top-to-south thrusts and folds; north-dipping foliation [29].</p>
	<p>Magmatism</p> <p>*See map for U-Pb ages (h,i). *Shallow level granitoids cross-cut slates. Age of intrusion interpreted from ⁴⁰Ar/³⁹Ar ages (h) 185±2 Ma [8], (i) 190±8 and 177±3 Ma [7].</p>	<p>*Bayan Har slate belt intruded by an undeformed tonalite with a Late Triassic K-Ar age [23].</p>
References	<p>1. Sengör and Okurogullari 1991 2. Sengör and Natal'in 1996 3. Cowgill, 2001 4. Laveine et al., 1996 5. Xinjiang Bureau of Geology and Mineral Resources, 1993 6. Liu, 1988 7. Matte et al., 1996 8. Xu, et al., 1996 9. Arnaud, 1992 10. Gilder et al., 1996 11. Yuan et al., 2002 12. Peltzer et al., 1989</p>	<p>13. Ryerson et al., 1999 14. Pan, 1996 15. Deng, 1996 16. Pan, 1990 17. Mattern et al., 1996 18. Yin and Harrison, 2000 19. Yao and Hsü, 1992 20. Dewey et al., 1988 21. Yin et al., 1988 22. Xu and Harris, 1990 23. Harris et al., 1988 24. Leeder et al., 1988 25. Kidd and Molnar, 1988 26. Van der Woerd et al., 1998 27. Van der Woerd et al., 2000 28. Molnar et al., 1987a,b 29. Coward et al., 1988 30. Watson et al., 1987</p>

Figure 4b. Summary of similarities in the geologic evolution of the two belts.

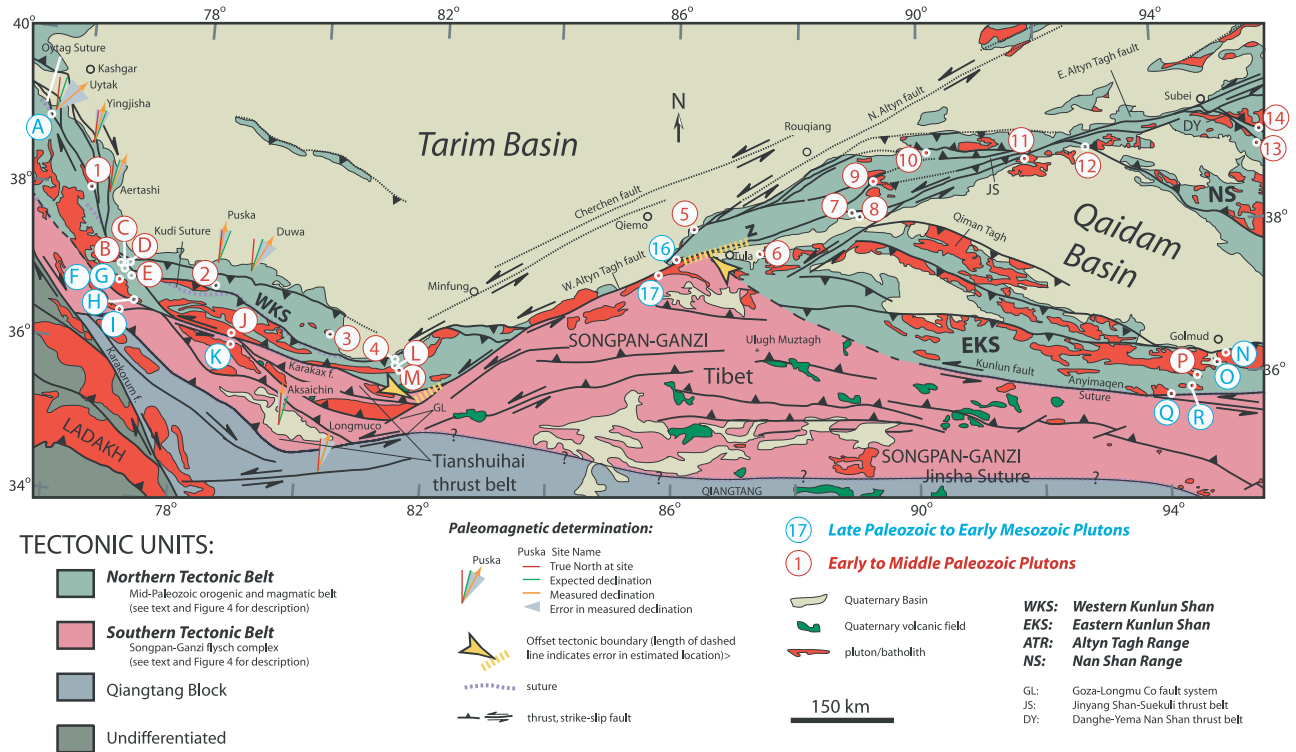


Figure 5. Tectonic map of the northwestern Tibetan Plateau showing offset tectonic boundary. Map was derived from data compiled in Figures 3 and 4. Offset tectonic boundary lies between a northern tectonic belt, consisting of a Cambro-Devonian magmatic province, and a southern tectonic belt, consisting of Songpan-Ganzi flysch. Location of boundary is fixed by pluton intrusive ages. Yellow arrows indicate 475 km offset of the tectonic boundary along the Altyn Tagh fault system, with dashed lines indicating ± 70 km error. See text for discussion. Paleomagnetic directions measured from Cretaceous and early Tertiary strata are also shown. Measured declinations generally overlap within error with those expected from the Eurasian apparent polar wander path [Besse and Courtillot, 1991] (Table 4). Where differences in measured and expected directions suggest vertical axis rotation (e.g., Uytak), such rotation generally appears to be due to local structures rather than regional tectonics [Chen *et al.*, 1992; Yin *et al.*, 2000].

dition of these tectonic provinces is significant because they are separated by a sharp, east-west striking boundary that has been offset by 475 ± 70 km along the Altyn Tagh fault (Figure 5). This offset determination is similar to those proposed by Ritts and Biffi [2000] and Chen *et al.* [2002].

[22] Although a comprehensive discussion of the geology of the western and eastern Kunlun Shan is beyond the scope of this paper, essential aspects of these two areas are summarized in Figures 4a and 4b. The defining characteristics of the northern tectonic belt, the tectonic boundary, and the southern tectonic belt are listed in Figure 4b from top to bottom, respectively. Geologic relations from the western and eastern Kunlun Shan are also given.

4.2.1. Northern Tectonic Belt

[23] Figure 4 indicates that the northern tectonic belt is an early to middle Paleozoic orogenic and plutonic complex that formed along the southern margin of the Tarim-North China craton. This early phase of plutonism was followed by a magmatically quiet period during which basement rocks were first exhumed during the development of regional unconformities and then buried by dominantly terrestrial deposits.

4.2.2. Southern Tectonic Belt

[24] In contrast to the northern belts, Figure 4 indicates that regions to the south are dominated by low-grade,

Permo-Triassic slate belts of the Songpan-Ganzi complex that accreted to Eurasia during closure of the Paleotethys ocean basin [Sengör, 1984; Sengör *et al.*, 1996; Sengör and Okurogullari, 1991]. These monotonous rocks are penetratively deformed by south vergent folds and are intruded by shallow level plutons [Matte *et al.*, 1996]. Several recent papers [Xiao *et al.*, 2002a, 2002b] have investigated the general tectonic setting of this belt in the western Kunlun Shan region.

4.2.3. Tectonic Boundary

[25] The boundary between the northern and southern tectonic belts is presently defined by the Karakax and Kunlun faults in the western and eastern Kunlun Shan, respectively. Both faults are active, left-lateral strike-slip faults that appear to have been superimposed upon an older suture zone, the Anyemaqen-Maqui or Kunlun suture [Dewey *et al.*, 1988]. This tectonic boundary also represents an abrupt contrast in metamorphic grade, with higher-grade rocks intruded by the Kunlun batholith exposed to the north.

[26] It is important to accurately locate this boundary because it is a discrete regional marker that can be used to determine total offset along the Altyn Tagh fault system. The tectonic map in Figure 5 shows the location of the tectonic boundary as interpreted from the regional geology

summarized in Figure 4 and the southernmost extent of samples from the older intrusive suite. In the eastern Kunlun Shan, samples 6 and 17 (Figure 3) provide a critical constraint on the position of the boundary on the southeast side of the Altyn Tagh fault system. These samples lie within 10 km of the active trace of the Altyn Tagh fault and indicate that the boundary between the northern and southern tectonic belts must lie between them. In the western Kunlun Shan, to the northwest of the Altyn Tagh system, the boundary lies southwest of samples L, M, and 4 and is bracketed by samples J and K. The arrowheads in Figure 5 indicate the tectonic boundary has been offset 475 ± 70 km along the Altyn Tagh fault.

[27] Do the present exposures in the western Kunlun Shan truly reflect the position of the tectonic boundary between the Paleozoic belt in the north and the Songpan-Ganzi flysch belt to the south? Although the following two scenarios are possible, in both cases the 475 ± 70 km offset is a minimum since the tectonic boundary would have originally been located south of its present position. One scenario is that the Songpan-Ganzi complex extends to the north beneath the Paleozoic belt. Because the Paleozoic belt is generally older than the Songpan-Ganzi complex, this older-on-younger configuration would require that the contact between the two belts is a north dipping thrust fault. In this case the southern edge of the hanging wall was originally located at, or to the south, of the present trace of the tectonic boundary. A second scenario is that the Paleozoic belt extends to the south, under the Songpan-Ganzi complex. In this case, the flysch belt was either obducted or deposited onto the southern edge of the Paleozoic basement. This scenario is unlikely since Permo-Triassic strata exposed within the Hotan thrust belt along the northern edge of the western Kunlun Shan (Figure 4) [Cowgill, 2001] do not correlate with the Songpan-Ganzi complex, indicating that such onlap cannot extend very far north of the present boundary. Also, the exposed boundary in the western Kunlun Shan appears to be a suture zone [Deng, 1996; Pan, 1996b; Yin and Harrison, 2000].

[28] Several factors contribute to the ± 70 km uncertainty in the proposed offset. The largest contribution results from ambiguity in the location of the intersections between the Altyn Tagh fault system and the tectonic boundary. North of the fault, in the western Kunlun Shan, the boundary curves into the fault (Figure 5). Depending on how the boundary is projected along strike, the location of the intersection varies by 45 km. South of the fault, in the eastern Kunlun Shan, the intersection lies between samples 6 and 17 (Figure 5). Although these samples lie ~ 150 km apart, field mapping [Cowgill, 2001] suggests that the pluton sampled at 17 continues ~ 50 km east, reducing the interval to ~ 100 km (Figure 5). The ± 70 km uncertainty in our total offset determination results from the combination of the ± 45 and ± 100 km uncertainties.

[29] A second source of uncertainty is the planar nature of the offset boundary. Although intersection of the boundary and the Altyn Tagh fault forms a piercing line, rather than a piercing point, two arguments suggest that this uncertainty is not significant. First, both the fault [Cowgill, 2001] and the boundary [Matte et al., 1996; Mattern et al., 1996] dip steeply. The piercing line is thus nearly vertical. Second, $^{40}\text{Ar}/^{39}\text{Ar}$ analyses [Arnaud, 1992; Cowgill, 2001] suggest

that broadly similar crustal levels are exposed adjacent to the fault in the western and eastern Kunlun Shan. We estimate that the error introduced by correlation of a piercing line is less than ~ 50 km.

[30] A third contribution to the uncertainty results from the possibility that offset of the tectonic boundary was produced by a transform segment in the mid-Paleozoic arc, Mesozoic slip along the Altyn Tagh system [e.g., Delville et al., 2001; Sobel et al., 2001], or oroclinal bending of the tectonic boundary. Although it is difficult to quantify these uncertainties, we argue that such errors can be neglected because these scenarios are unlikely. It is unlikely that separation reflects an original transform segment because deformation at the southwest end of the Altyn Tagh system appears to postdate Mesozoic accretion of the Qiangtang and Lhasa blocks. In addition, offset of a Tertiary thrust belt by ~ 380 km along the eastern Altyn Tagh fault [Yin and Harrison, 2000] indicates that a significant fraction of the 475 ± 70 km total offset is Cenozoic. Finally, it is unlikely that the separation between the western and eastern Kunlun Shan results from oroclinal bending, since the tectonic boundary approaches the fault system at a high angle.

4.3. Incompatibility With Existing Models

[31] Left slip on the Altyn Tagh system is generally thought to have been absorbed by underthrusting [Avouac and Peltzer, 1993; Matte et al., 1996] and possibly south dipping subduction [Arnaud, 1992; Mattauer, 1986; Matte et al., 1996] of Tarim along the northern margin of the western Kunlun Shan. The Tiklik and Hotan faults (Figure 4) clearly attest to north directed thrusting along this margin [Avouac and Peltzer, 1993; Cowgill, 2001; Matte et al., 1996]. However, this structural configuration cannot account for the 475 ± 70 km offset of the tectonic boundary.

[32] As Figure 6a indicates, the problem with the present structural configuration is that it places both the western and eastern Kunlun Shan belts in the same plate. As Figure 6b indicates, displacement of the tectonic boundary requires that the western and eastern Kunlun Shan batholiths were originally located within separate plates so that the eastern Kunlun Shan and Tibet could move to the east-northeast relative to the western Kunlun Shan and Tarim. Thus offset of the western and eastern Kunlun Shan requires that a major fault system lies to the south of the western Kunlun batholith.

[33] One possibility is that this structure is a strike-slip fault. In this case, offset of the tectonic boundary is due to eastward extrusion of the Tibetan Plateau via simultaneous slip on the conjugate Karakorum and Altyn Tagh/Karakax faults [Molnar and Tapponnier, 1978; Peltzer and Tapponnier, 1988; Tapponnier et al., 1982]. However, there are three problems with this model. First, the total offset along the southern Karakorum fault ranges from ~ 120 km [Searle, 1996] to only ~ 60 km [Murphy et al., 2000], limiting the extent to which this fault could have accommodated enough eastward extrusion to create the asymmetry of the Tibetan Plateau. Second, as Figure 7 indicates, the extrusion model predicts $\sim 35^\circ$ of clockwise, vertical axis rotation of the western Kunlun Shan and Karakax fault. Paleomagnetic directions measured from Cretaceous and early Tertiary strata north and south of the western Kunlun batholith (Table 4 and

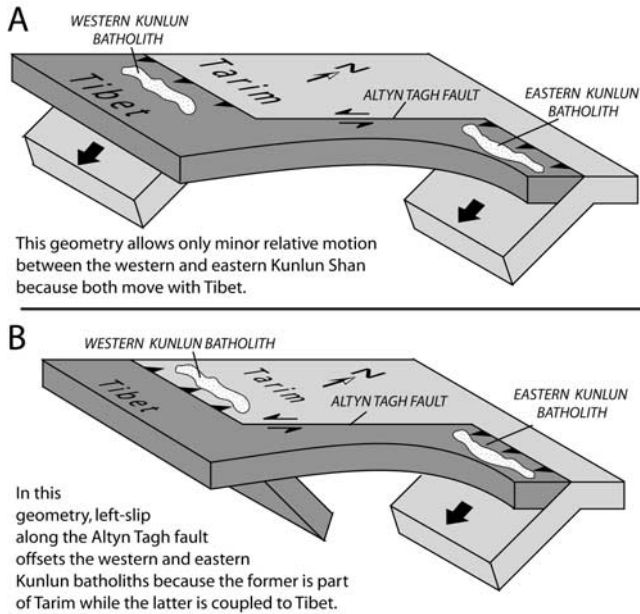


Figure 6. Schematic block diagrams showing possible geometry of Altyntagh-western Kunlun-Nan Shan/Qilian Shan fault system. (a) Altyntagh links south dipping thrusts in the western Kunlun Shan and the Nan Shan-Qilian Shan. This is the present configuration. In this geometry both the eastern and western Kunlun Shan lie in the upper plate. Therefore this structural configuration cannot account for offset of the tectonic boundary. (b) Altyntagh links north dipping thrusts in the hypothesized Tianshuihai thrust belt with south dipping thrusts in the Nan Shan-Qilian Shan. In this configuration the western Kunlun Shan moves with Tarim while the eastern Kunlun Shan moves with Tibet. We argue that this structural geometry offsets the tectonic boundary by 475 ± 70 km.

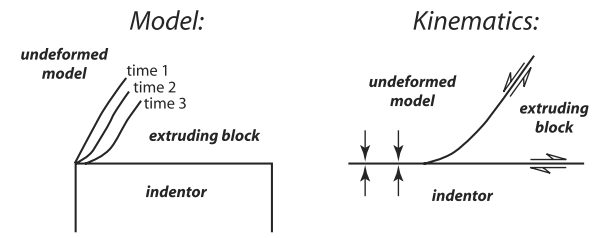
Figure 5) [Chen *et al.*, 1992, 1993; Gilder *et al.*, 1996; Rumelhart *et al.*, 1999; Yin *et al.*, 2000] are inconsistent with such rotation. Because rocks to the north and south of the western Kunlun belt have not been appreciably rotated, it is likely that the intervening Kunlun belt also has not been rotated. Finally, because the western and eastern Kunlun Shan have similar strikes, it is simpler to conclude that they were initially linear, rather than initially kinked (e.g., Figures 7b and 7c) and subsequently straightened by vertical axis rotation of the western Kunlun Shan (e.g., Figures 7d and 7e).

5. Discussion

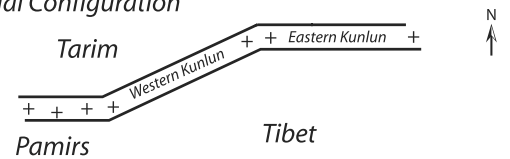
5.1. The Tianshuihai Thrust System

[34] To explain the offset of the tectonic boundary, we propose that left slip motion along the Altyntagh fault system was primarily accommodated at the southwestern end of the fault by the Tianshuihai thrust system, a south directed thrust belt that we suggest lies to the south of the western Kunlun batholith (Figures 6b and 8). We refer to this system as a back thrust belt because deformation within this thrust belt was directed into the interior of the Tibetan orogen. As discussed below, there are two essential aspects

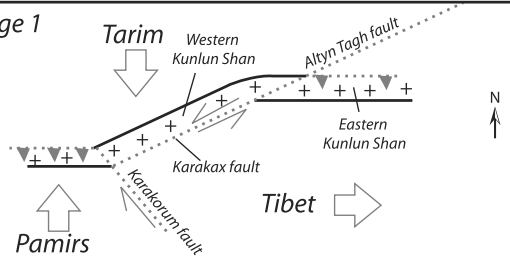
(A) Fault Rotation in Analog Models:



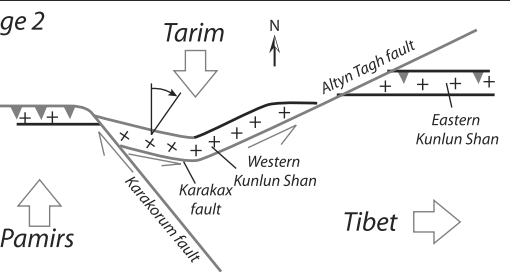
(B) Initial Configuration



(C) Stage 1



(D) Stage 2



(E) Present

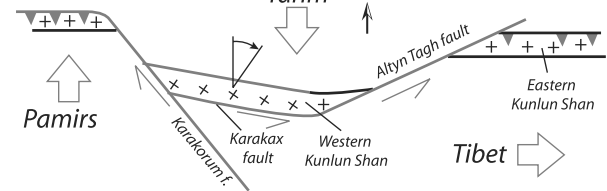


Figure 7. Predictions of the lateral extrusion model. (a) Diagram showing clockwise fault rotations as observed in analog models of extrusion. Such rotations have been cited to explain the change in strike between the Altyntagh and Karakax faults [Peltzer and Tapponnier, 1988]. The position and geometry of the fault separating the undeformed model from the extruding block is shown at three different times (t_1 , t_2 , and t_3) and indicates that the fault rotates clockwise as extrusion progresses (diagram modified from Peltzer and Tapponnier [1988]). (b–d) Predicted evolution of the western Kunlun Shan. The extrusion model predicts that the original strike of the western Kunlun Shan batholith and the Karakax fault was $\sim 070^\circ$ (i.e., parallel to the central section of the Altyntagh fault) prior to extrusion. The model also predicts that during extrusion both the batholith and the Karakax fault sequentially rotated $\sim 35^\circ$ clockwise into their present $\sim 105^\circ$ trend.

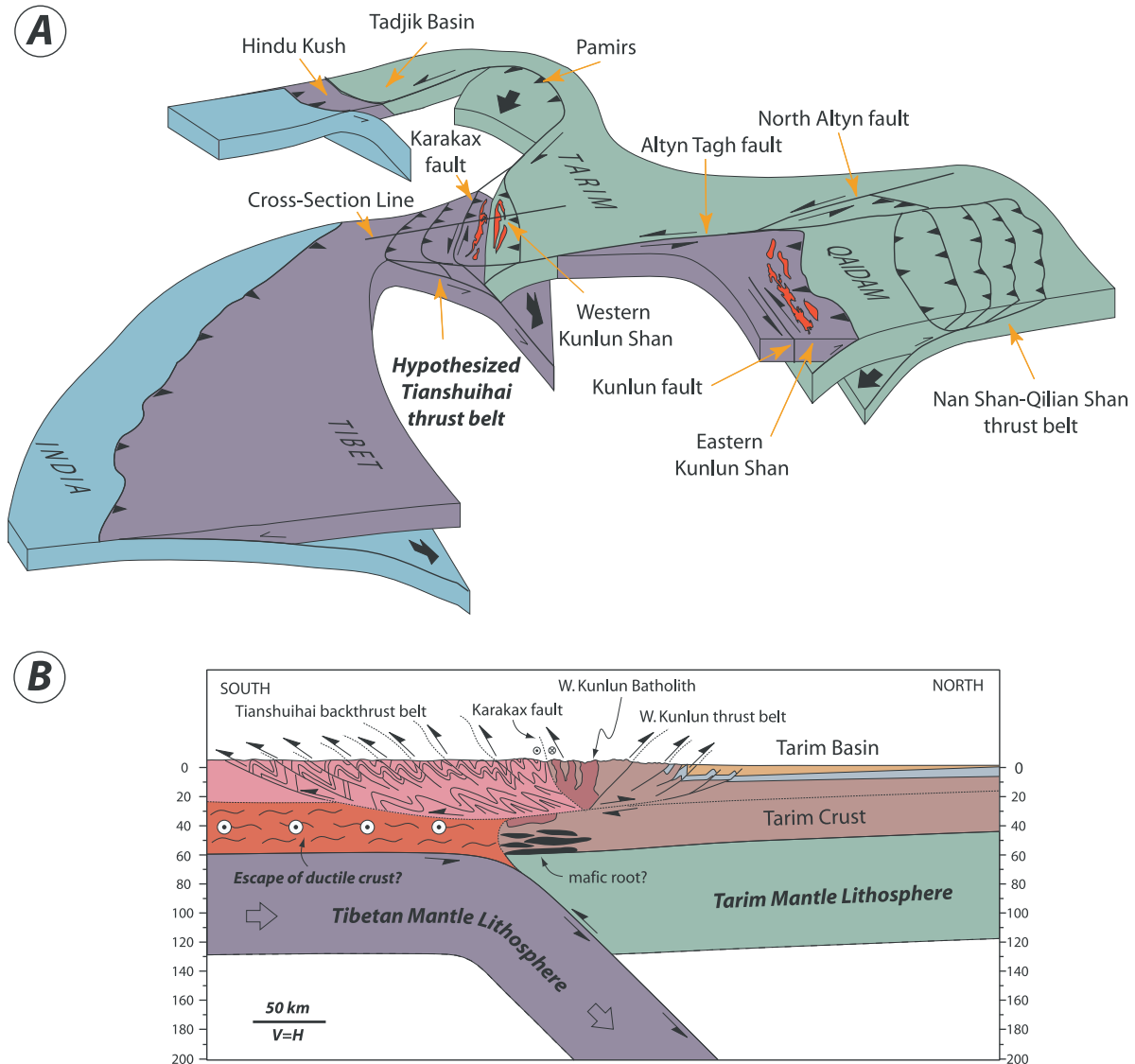


Figure 8. Diagrams showing major structures within the northern Tibetan Plateau and the proposed structural geometry at the southwest end of the Altyn Tagh fault system. (a) Three-dimensional perspective diagram. We hypothesize that 475 ± 70 km of left separation between the western and eastern Kunlun Shan was accommodated at the western end of the Altyn Tagh fault by south directed thrusting along the Karakax fault and within the Tianshuihai thrust belt. Plates represent continental lithosphere. The extent to which continental crust has been subducted within these thrust belts remains to be determined. View is to the west-northwest. (b) Schematic lithospheric-scale cross section through western Tibet and the western Kunlun Shan showing the geometry of the proposed south directed thrust system. To account for the offset between the western and eastern Kunlun Shan, we propose that shortening was accommodated in the upper crust by a south directed thrust belt, in the middle/lower crust by east directed flow of weak crust, and in the mantle lithosphere by north directed subduction.

tightly folded Jurassic terrestrial deposits [Matte *et al.*, 1996] indicating that this deformation is younger than Middle Jurassic. Within the Songpan-Ganzi flysch complex, some of the folds between Mazar and Kangxiwar (Figure 4) are south vergent, as are isoclinal folds in the vicinity of Aksai Chin (Figure 5) [Matte *et al.*, 1996]. Aureoles around Jurassic plutons locally overprint cleavage within the slate belt [Matte *et al.*, 1996] indicating that at least some of this deformation is pre-Tertiary in age. However, two phases of folding are evident in the Bazar Dara slates [Gaetani *et al.*,

1990]. We suspect that the extent and magnitude of the younger phase of deformation have not been fully appreciated due to the paucity of marker beds and the south vergent nature of both phases of deformation.

[40] A regionally extensive back thrust system defines the leading edge of the Altiplano-Puna Plateau and indicates that the hypothesized Tibetan back thrust system is feasible. The Altiplano-Puna segment of the South American Andes is the second largest plateau on Earth. West directed back thrust systems define the eastern edges of the Altiplano

[McQuarrie and DeCelles, 2001; Roeder, 1988] and Puna [Grier et al., 1991] sections of the plateau and continue to the south into the basement uplifts of the Santa Barbara [Allmendinger and Gubbels, 1996] and Sierras Pampeanas ranges [Jordan and Gardeweg, 1989; Jordan et al., 1983]. These back thrusts are thought to root into a master detachment at depth [see Allmendinger and Gubbels, 1996; Grier et al., 1991; McQuarrie and DeCelles, 2001].

5.2. Evolution of the Altyn Tagh System

[41] In Figure 9 we have reconstructed the Cenozoic evolution of the Altyn Tagh system and its adjacent thrust belts to illustrate how this system might have evolved. This reconstruction illustrates that offset estimates for individual structures within the Altyn Tagh-western Kunlun system can be combined to balance deformation along the northern margin of the Tibetan Plateau.

[42] To reconcile early, south directed thrusting in the western Kunlun Shan region with the present north directed deformation, we suggest that Cenozoic left slip along the Altyn Tagh fault has been accommodated by two stages of deformation (Figure 9). In the first phase, deformation at the southwestern end of the fault system was dominated by south directed thrusting in the Tianshuihai thrust belt. In the second stage, deformation switched to dominantly north directed thrusting along the northern margin of the range. The extent to which these thrust systems were active simultaneously is unclear. One possibility is that cessation of south directed thrusting in the Tianshuihai belt coincided with the initiation of north directed thrusting along the Hotan and Tiklik faults (Figure 4). However, it is more likely that both thrust systems were active simultaneously and that a drop in the shortening rate of the Tianshuihai belt coincided with an increase in the shortening rate to the north. In either case, we suspect that the reversal in thrust polarity was triggered by uplift of the Tibetan Plateau.

[43] From the Eocene to the late Miocene (Figure 9), we infer that left slip on the Altyn Tagh fault was accommodated at the western end of the fault primarily by the Karakax fault and north dipping thrusts within the Tianshuihai thrust belt to the south. In contrast, slip at the eastern end of the fault was accommodated by south dipping thrusts within the Nan Shan and Qilian Shan. As a result of this geometry, the eastern Kunlun Shan was coupled with Tibet and both moved northeast relative to the western Kunlun Shan that formed part of Tarim. Separation between the western and eastern Kunlun Shan accumulated while this structural configuration was active (see Figure 6b).

[44] Between the Eocene and Oligocene (Figure 9), thrusting initiated within the Qiman Tagh and the composite Jinyang/Suekuli-Danghe/Yema Nan Shan thrust belt farther north [Gehrels et al., 1999; Yin and Harrison, 2000]. These north directed thrust belts were probably initially linked to the south directed Karakax fault and Tianshuihai thrust belt via the North Altyn and possibly the Cherchen faults [Cowgill et al., 1997; Yin and Harrison, 2000].

[45] Between Oligocene to late Miocene, the Tula-Subei segment of the Altyn Tagh fault formed (Figure 9), cutting the Jinyang/Suekuli-Danghe/Yema Nan Shan thrust belt and initiating left separation of the two halves of this Tertiary thrust belt [Gehrels et al., 1999; Yin and Harrison, 2000]. Slip along the North Altyn fault either fed back into the

Tula-Subei segment of the Altyn Tagh fault as part of a rhomb-shaped transpressional duplex [Cowgill et al., 2000] or it continued into Mongolia, linking with left slip faults described by Lamb et al. [1999].

[46] North directed thrusting along the northern edge of the western Kunlun Shan had initiated at or prior to ~ 37 Ma [Rumelhart, 1998]. We interpret this thrust system to have initiated as a conjugate to the main, south directed Tianshuihai thrust belt. In this interpretation, most of the Oligo-Miocene relative motion between Tarim and Tibet was accommodated by shortening within the Tianshuihai thrust belt. As deformation progressed, it appears that north directed faulting within the western Kunlun thrust belt accelerated at the expense of shortening within the Tianshuihai thrust belt (Figure 9). This kinematic reorganization of the west Kunlun-Altyn Tagh structural system transferred the western Kunlun Shan from the Tarim block to the Tibetan Plateau, thereby terminating large-magnitude relative motion between the western and eastern Kunlun Shan (Figures 6 and 9).

[47] We estimate the total offset along the Minfung-Qiemo section of the western Altyn Tagh fault (Figure 5) to be ~ 575 km. This value combines the Tibet-Tarim offset that was absorbed by ~ 100 km of north directed thrusting along the Hotan and Tiklik faults (Figure 4) [Cowgill, 2001; Lyon-Caen and Molnar, 1984] and 475 ± 70 km of offset of the tectonic boundary. East of Qiemo (Figure 5), structural mapping indicates that rocks on opposite sides of the North Altyn fault do not match for ~ 120 km along strike, suggesting that left slip separation is at least this large [Cowgill et al., 2000]. Some of this strike-slip deformation may have been responsible for the initial development of the Jinyang/Suekuli-Danghe/Yema Nan Shan thrust belt. This thrust belt has subsequently been dissected and offset by an additional 280 ± 30 km along the Tula-Subei segment of the eastern Altyn Tagh fault (Figure 5) [Yin and Harrison, 2000]. Total offset on the Qiemo-Subei section of the eastern Altyn Tagh fault system is thus ~ 400 km, equivalent to the offset determined from correlation of a Jurassic facies boundary across the fault [Ritts and Biffi, 2000]. In our reconstruction (Figure 9), 180 km of shortening within the Qiman Tagh accounts for the eastward decrease in offset between the Minfung-Qiemo and Qiemo-Subei segments of the Altyn Tagh fault system.

[48] Previous work in the North Pamir and Paropamisus blocks (Figure 1c) [e.g., Boulain, 1988; Girardeau et al., 1989; Stöcklin, 1989] suggests that the tectonic boundary continues west of the Kunlun Shan [Burtman and Molnar, 1993; Sengör, 1984]. The boundary appears to coincide with the Akbaytal and Herat faults in the North Pamirs and Afghanistan, respectively (Figure 1c). By the late Miocene, indentation of the Pamir syntaxis had begun to deform the western section of the Kunlun-Tianshuihai belt (Figure 9). Southward subduction of the Tarim-Tadjik crust beneath the Pamirs, as well as internal shortening within the syntaxis displaced the tectonic boundary 300+ km to the north [Burtman and Molnar, 1993]. We estimate that the boundary shows ~ 360 km of sinistral offset and ~ 270 km of dextral offset along the western and eastern sides of the Pamirs, respectively (Figure 9). The mapped pattern of deformation suggests that oroclinal bending has accommodated a significant fraction of this displacement with the

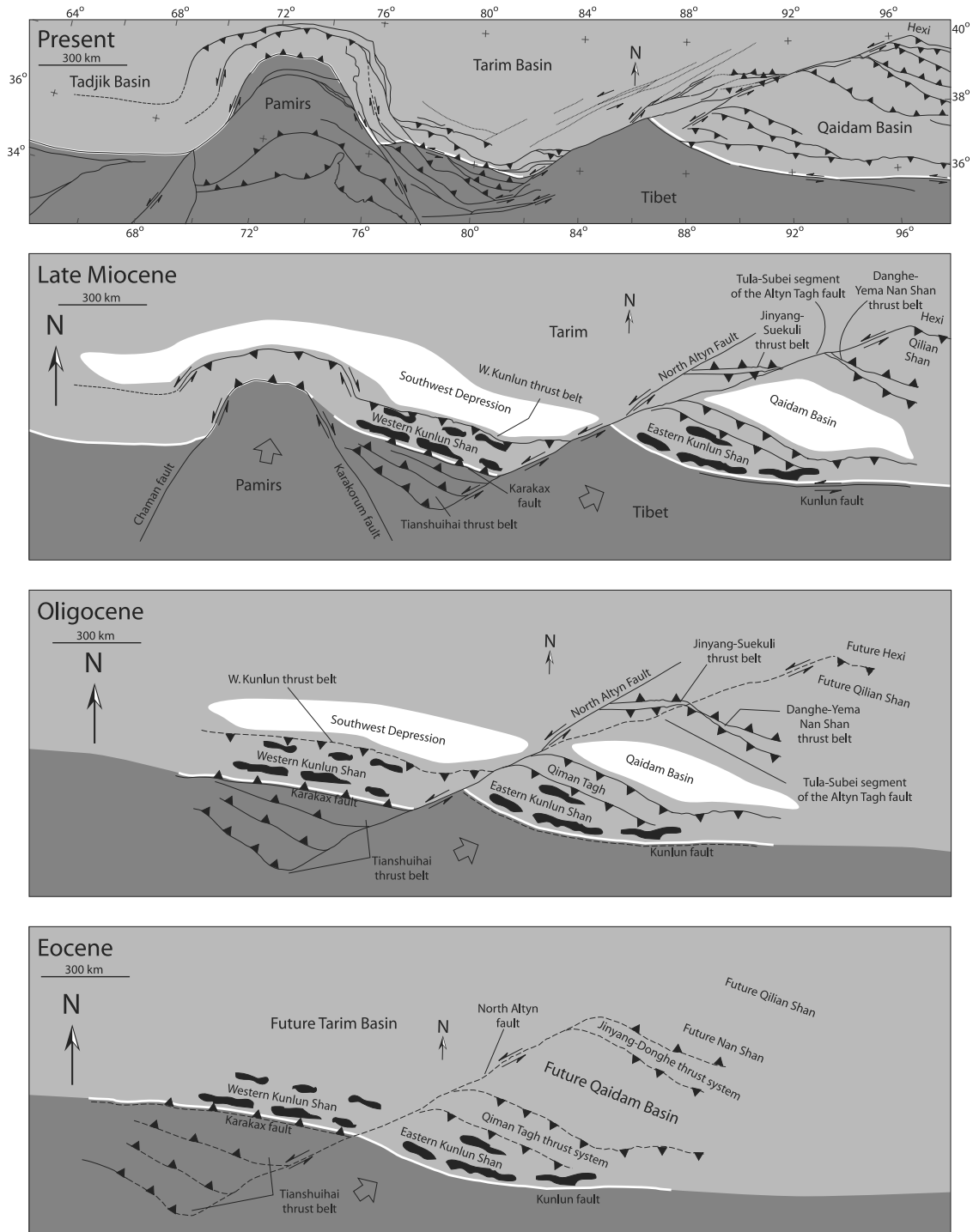


Figure 9. Reconstruction of Tertiary deformation within the western Kunlun-Altyr Tagh-Nan Shan system. See text for discussion. White line shows boundary between the two tectonic belts. White areas indicate foreland basins and black regions indicate batholiths. Dashed faults are inactive. Because the detailed evolution of the thrust belts is unknown, we simply show the belts as shortening and do not show deformation propagating toward the foreland. Open arrows indicate approximate motion relative to fixed Tadjik-Tarim-Hexi block. The “present” fault geometry was compiled from references listed in caption to Figure 1c.

remainder occurring as slip along the Chaman and Karakorum fault systems (Figure 9). Total offset on the east side of the syntaxis is ~ 90 km less than on the west side because the west Kunlun thrust belt has moved north relative to both

the Tarim and Paropamisus along the north directed Kunlun thrust system.

[49] It is possible to calculate the long-term slip rate of the Altyr Tagh fault system by combining the total offset on

the Altyn Tagh system with estimates of its initiation age. Several lines of evidence indicate that the Altyn Tagh fault system had begun to develop by at least 37 ± 5 Ma, including magnetostratigraphic constraints on the timing of the onset of coarse-clastic deposition within the Tarim Basin [Rumelhart, 1998; Yin *et al.*, 2002], apatite fission track data from the western Kunlun Shan and Altyn Tagh [Cowgill, 2001; Rumelhart, 1998; Sobel, 1995; Sobel *et al.*, 2001; Yin *et al.*, 2002], and the timing of reorganization of sediment dispersal patterns within the northwestern Qaidam basin [Hanson, 1997]. A mid-Oligocene initiation age for the central Altyn Tagh fault is also consistent with cooling histories derived from interpreting $^{40}\text{Ar}/^{39}\text{Ar}$ K-feldspar results in the context of multidiffusion domain theory [Cowgill *et al.*, 2001].

[50] By combining this initiation age with our total offset estimate of 475 ± 70 km we calculate a 37 Ma average slip rate of 13 ± 3 mm/yr. This rate is equivalent, within error, to rates determined from a recent global positioning system (GPS) study (9 ± 2 mm/yr) [Shen *et al.*, 2001], and is consistent with results from a recent paleoseismic study of the central Altyn Tagh fault [Washburn *et al.*, 2001]. As discussed above, the total offset across the western Altyn Tagh fault system (between Minfung and Qiemo in Figure 5) is estimated to be ~ 575 km, in which case the long-term slip rate of the system as a whole is 16 ± 3 mm/yr.

6. Implications

6.1. Structural Style as a Function of Depth

[51] If the Tianshuihai back thrust hypothesis is correct, then the following mass balance indicates that a significant volume of crust has been removed from western Tibet during Cenozoic shortening. According to the back thrust hypothesis, the Tianshuihai thrust belt has accumulated ~ 475 km of shortening. Since this belt is presently ~ 200 km wide, its original width must have been ~ 675 km indicating that the belt has been shortened by $\sim 68\%$. Because the present crustal thickness of the inferred thrust belt is ~ 63 km [Ma, 1980], northeast-southwest sections across the belt have an area of $\sim 12,600$ km². The original crustal thickness can be calculated using the observation that widespread limestones near Aksai Chin and the Ghoza-Longmu Co (Figure 5) [Matte *et al.*, 1996; Norin, 1946] were deposited near sea level between the Aptian and Cenomanian [Matte *et al.*, 1996]. By assuming that these rocks were uplifted to their present elevation of 5000+ m by Airy isostatic compensation of regionally thickened crust, we calculate [e.g., Turcotte and Schubert, 1982, equation 5.146] that the crust was ~ 30 km thick when they were deposited. In this case, northeast-southwest cross sections across the 675 km wide belt had an initial area of $\sim 20,250$ km². Comparison of initial and final sections indicates $\sim 40\%$ of the original crustal thickness has been lost from western Tibet.

[52] Although the simplest explanation is that the excess mass has been removed by erosion, this is unlikely since it would produce widespread exposures of midcrustal rocks in western Tibet, rather than the observed slates of the Tianshuihai belt. A second possibility is that the excess crust has been removed by the subduction of either remnant oceanic lithosphere or dry lower continental crust.

As described below, the Songpan-Ganzi complex accreted to the southern margin of Eurasia during doubly vergent subduction of the Paleotethys ocean basin [e.g., Sengör, 1984; Sengör and Natal'in, 1996]. If Mesozoic subduction was incomplete, then prior to the onset of the Indo-Asian collision the Tianshuihai complex would have been underlain by a relict oceanic slab that was trapped between the Lhasa-Qiangtang blocks to the south and the Tarim-North China blocks to the north. The Black and Caspian Seas are essentially modern analogues for such a setting, although Cretaceous shallow marine deposits in western Tibet suggest that the Paleotethys basin had been filled with sediment prior to the Indo-Asian collision. Reactivation of subduction during Cenozoic shortening could then remove the oceanic crust that floored this basin. The lack of extensive subduction-related volcanics in southern Tarim and western Tibet requires a mechanism for rejuvenating subduction without producing an associated volcanic arc. However, if Mesozoic subduction completely removed the oceanic lithosphere during hidden subduction [i.e., Sengör, 1984], then the asthenosphere could have been emplaced against the base of the accretionary complex, causing it to undergo widespread dehydration. Dry, metasedimentary xenoliths of the lower crust in central Tibet [Hacker *et al.*, 2000a] may have formed by such a process. Subduction of dry lower crust may account for the loss of mass from western Tibet without the construction of a magmatic arc. Although in these subduction scenarios the Tianshuihai complex is underlain by either relict oceanic crust or dehydrated metasediments, another likely scenario is that most of the crust consists of the same hydrous, quartz-dominated lithologies exposed in western Tibet, and a similar crustal structure has been proposed for central Tibet [Kapp *et al.*, 2000]. According to the compilation of flow laws reported by Carter and Tsen [1987], crust that is dominated by wet, quartz-rich lithologies will have minimal strength (<10 MPa) below 12 km depth for a typical continental geotherm and a strain rate of 10^{-14} s⁻¹ [see also Brace and Kohlstedt, 1980; Molnar, 1992; Ranalli and Murphy, 1987]. Thus a third possibility is that the excess crust of western Tibet was removed by ductile flow of a weak middle/lower crust. Due to the narrow north-south width of the Pamirs (Figure 1), this crust may have been expelled eastward, helping to inflate the central Tibetan Plateau (Figure 8b). Weak middle to lower crust beneath the Tibetan Plateau has also been inferred from geophysical studies [Nelson *et al.*, 1996 and references therein] and geodynamic models that incorporate a depth-dependent viscosity [Clark and Royden, 2000; Royden, 1996; Royden *et al.*, 1997; Shen *et al.*, 2001]. To balance the ~ 500 km of crustal shortening at depth, we suggest that the "Tibetan" (i.e., Qiangtang and Songpan-Ganzi) mantle lid was subducted northward beneath Tarim (Figure 8b).

6.2. Why Did the Tianshuihai Back Thrust System Form?

[53] Above we argue that Cenozoic left slip along the Altyn Tagh fault system has been absorbed at the southwestern end of the fault by thin-skinned, south directed thrusting within the Tianshuihai slate belt. Structures inherited from the Paleozoic and Mesozoic assembly of

Eurasia appear to have been important in controlling the development of this system.

[54] Figure 10 showing the pre-Cenozoic evolution of the Songpan-Ganzi flysch belt to illustrate this point. By the early Mesozoic (Figure 10a) the composite Tarim-Qaidam-North China block represented the southern margin of Laurasia [Sengör and Natal'in, 1996; Yin and Nie, 1996]. Protoliths of the Songpan-Ganzi flysch belt accumulated as a subduction-accretion complex and forearc basin during Late Permian-Early Triassic north directed subduction of the

Paleotethys ocean crust beneath this margin [Matte et al., 1996; Sengör, 1984; Sengör and Natal'in, 1996; Sengör and Okurogullari, 1991; Watson et al., 1987; Yin and Harrison, 2000; Yin and Nie, 1996]. North directed subduction ended in the Middle to Late Triassic (Figure 10b) following collision between the North and South China continents along the Qinling-Dabie orogenic belt and partial subduction of the South China continent [see Hacker et al., 2000b and references therein; Hacker et al., 1996; Nie, 1991]. In the Late Triassic to Early Jurassic (Figure 10c), south directed subduction of the Paleotethys ocean crust beneath the Qiangtang closed the Paleotethys ocean basin [Dewey et al., 1988; Sengör, 1984; Sengör and Natal'in, 1996; Sengör and Okurogullari, 1991] and trapped the Songpan-Ganzi flysch complex [Sengör, 1984] and remnant ocean basin [Yin and Nie, 1993, 1996] in the interior of the Eurasian continent.

[55] Two aspects of this history appear to be particularly significant with respect to the development of the Tianshuihai back thrust system. First, we suggest that termination of north directed subduction in the Triassic produced a north dipping suture within the mantle lithosphere beneath the western Kunlun Shan that reactivated during the Indo-Asian collision. It is likely that the upper plate of this mantle suture zone consisted of hydrated mantle, while the suture itself could have been coated with serpentinites and possibly metasedimentary units that had been plated onto the walls of the subduction thrust. If these materials were present, then it is possible that the mantle suture could have remained a plane of weakness following closure of the Paleotethys ocean basin. If such a relict suture has been reactivated within the western Kunlun Shan, then it suggests such sutures may remain weak for more than 200 Myr following their formation. The longevity of such a weakness may result from the compositional changes produced by hydration of the upper plate mantle during prolonged subduction of oceanic lithosphere. It is possible therefore that the longevity of such weak sutures may be controlled by the intensity of upper plate alteration, and thus the duration of subduction, that preceded formation of the suture.

[56] Second, during reactivation of the mantle suture it appears that the Tianshuihai back thrust system developed by propagation of deformation away from the strong Tarim lithosphere and into the weaker Songpan-Ganzi flysch belt. The continuity of Phanerozoic deposits within the Tarim Basin indicates that the basin has been little deformed since the late Paleozoic [Jia, 1997; Li et al., 1996; Sengör et al., 1996] and attests to the strength of the Tarim lithosphere.

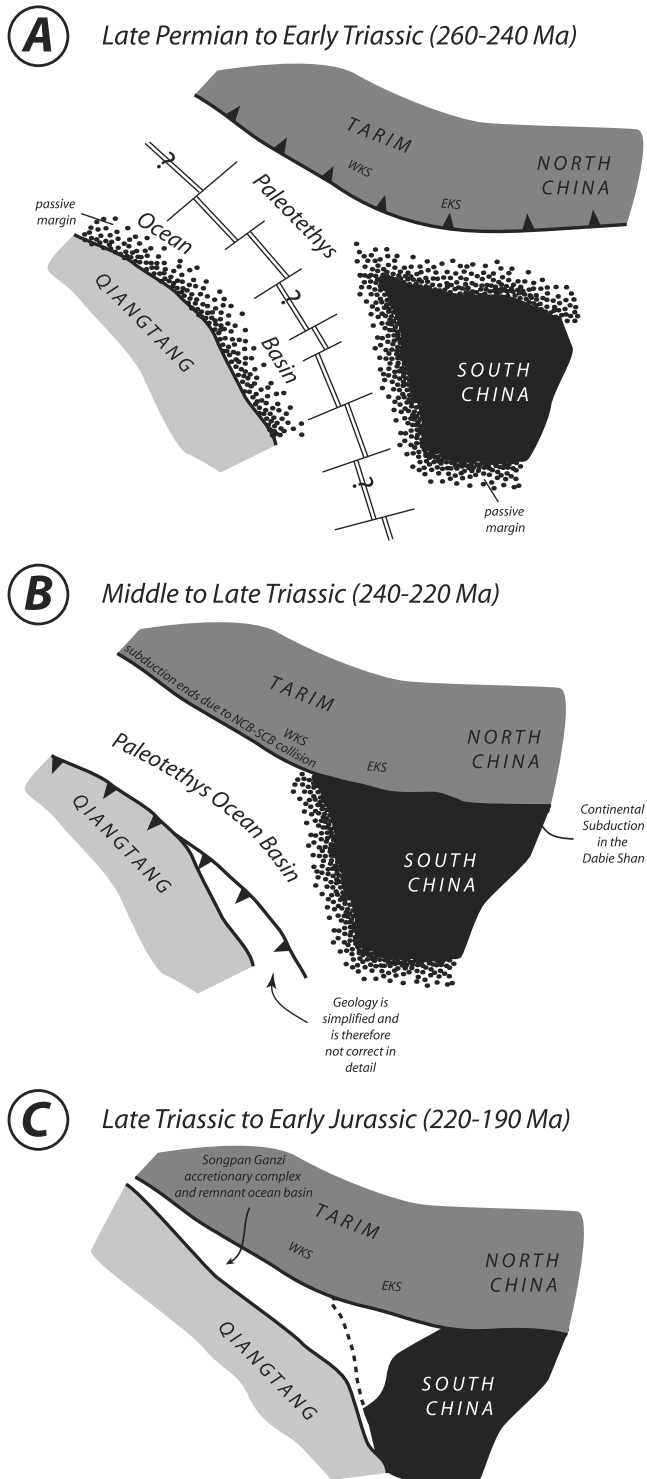


Figure 10. (opposite) Schematic block diagrams showing proposed pre-Cenozoic tectonic evolution of the Kunlun Shan. We propose that closure of the Paleotethys ocean produced a north dipping mantle suture beneath the western Kunlun Shan and accreted the weak Songpan-Ganzi flysch belt to the southern margin of the strong Tarim lithosphere. During the Indo-Asian collision, these lateral and vertical variations in strength appear to have played a fundamental role in controlling how the Eurasian continent deformed. Note that the tectonic evolution of the eastern part of the Songpan Ganzi region is greatly simplified for the sake of clarity. See the work of Sengör [1984] for a discussion on the tectonic evolution of this region.

By contrast, much of the deeper crust of the central Tibetan Plateau may be composed of weak Songpan-Ganzi mélangé that underplated the Qiangtang block during the Late Triassic [Kapp *et al.*, 2000]. Kapp *et al.* [2000] suggest that this mélangé may be weaker and wetter than the surrounding continental basement, thus explaining the high crustal Poisson's ratio [Owens and Zandt, 1997] and widespread Cenozoic volcanism of northern Tibet [Deng, 1978], as well as the more intense Cenozoic shortening in northern Tibet [Coward *et al.*, 1988] than in the Lhasa terrane to the south [Coward *et al.*, 1988; Murphy *et al.*, 1997]. Although deep crustal xenoliths are not consistent with present-day crustal melting in northern Tibet, they do indicate that the lower crust of Qiangtang is at least partly metasedimentary [Hacker *et al.*, 2000a]. Geodynamic models incorporating a strong Tarim basin region also show asymmetric plateau development [Neil and Houseman, 1997; Soofi and King, 2002].

6.3. What Controls Continental Deformation?

[57] Our reconstruction of the tectonic evolution of western Tibet and the Altyn Tagh fault system suggests that vertical and lateral variations in the strength of the Eurasian continental lithosphere played a first-order role in determining where, when, and how Indo-Asian convergence was absorbed to form the Tibetan Plateau. Above we present three hypotheses to explain 475 ± 70 km of left separation between the western and eastern Kunlun Shan. First, we suggest that western Tibet has been shortened by the south directed Tianshuihai back thrust belt at the southwestern end of the Altyn Tagh fault system. Second, we argue that shortening within this belt was accommodated in the upper crust by thin-skinned thrusting, in the mantle lithosphere by north directed subduction, and in the middle/lower crust by either east directed flow or subduction of relict oceanic basement or dry lower crust. Third, we propose that the back thrust system formed by reactivation of a north dipping mantle suture and localization of deformation in the weak Songpan-Ganzi complex rather than the stronger Tarim.

[58] If the factors controlling the geometry and evolution of Cenozoic deformation in western Tibet generally hold, then they lead to a conceptual model of crustal deformation that integrates key aspects of both the microplate and continuum views. In particular, the tectonics of western Tibet suggest that two parameters are key in controlling how a continent deforms in response to a given set of applied boundary conditions (1) the existence, geometry, and strength of sutures within the mantle lithosphere and (2) lateral variations in the strength of the middle to lower crust. The synthesized view is one in which plate tectonics holds in the mantle (microplate theory), but the upper crust may or may not track motion of underlying plates, depending on strength of middle to lower crust (continuum theory). Where the middle/lower crust is weak, the upper crust is detached, potentially allowing the crust to thicken by crustal inflation. In such cases, the kinematics of deformation in the upper crustal and mantle lithosphere will be decoupled. Where the middle/lower crust is strong enough to keep the upper crust firmly coupled to the mantle lid, upper crustal deformation does track deformation in the lower crust and upper mantle. Thus lateral variations in preexisting strength

of both the mantle and crust will play a profound role in controlling how continents deform.

7. Conclusions

[59] The following conclusions can be drawn from our investigation of the Altyn Tagh-western Kunlun fault system.

[60] 1. U-Pb ion microprobe analyses of zircons from 17 plutons from the northwestern margin of the Tibetan Plateau document a matching pair of plutonic belts in the western and eastern Kunlun Shan. A dominantly Ordovician belt is found only north of the Karakax and Kunlun faults while an Early Permian to Early Jurassic belt occurs both north and south of these structures.

[61] 2. Combining the timing of plutonism determined from zircon geochronology with thermochronologic and regional geologic data indicates that the matching plutonic belts coincide with a pair of tectonic provinces. The northern tectonic belt is an early to middle Paleozoic orogenic and plutonic complex that formed along the southern margin of the Tarim-North China craton. The southern tectonic belt is characterized by the Songpan-Ganzi flysch belt that was accreted to this margin upon closure of the Paleotethys ocean. These belts are separated by a sharp east-west striking boundary that has been offset by 475 ± 70 km along the Altyn Tagh fault.

[62] 3. Recent left-lateral slip along the Altyn Tagh system has been accommodated at the western end of the fault by north directed thrusting. However, it is unlikely that this structural system produced ~ 475 km offset between the western and eastern Kunlun Shan since both belts lie within Tibet. To explain offset of the western and eastern Kunlun Shan we propose that north directed faulting at the eastern end of the Altyn Tagh fault was initially mirrored by south directed back thrusting at the west end of the fault along the Karakax fault and Tianshuihai thrust belt. Tibet-Tarim convergence across these belts resulted in the extreme narrowing of both the Tibetan Plateau in western Tibet and the Tarim basin in the Hexi corridor.

[63] 4. Within the back thrust belt, upper crustal shortening within the hypothesized back thrust belt appears to have been accommodated by thin-skinned thrusting. To balance this shortening at depth we argue that the middle/lower crust of the Songpan-Ganzi complex and the Qiangtang block was either weak, and has been evacuated by east directed flow, or it was strong and was subducted into the mantle. One explanation for a strong lower crust is that it was a relict oceanic slab that floored a remnant ocean basin similar to the Black or Caspian Seas. Another possibility is that the lower crust was dry and strong due to metamorphism and/or partial melting extraction following foundering of the subducting slab during closure of the Paleotethys ocean basin. We suggest that shortening of the western Tibetan mantle lithosphere was accommodated by north dipping subduction.

[64] 5. Structures inherited from the late Paleozoic to Mesozoic assembly of Eurasia appear to play a critical role in dictating the style of deformation at the western end of the Altyn Tagh system. Specifically, we propose that the back thrust system formed by reactivation of a north dipping mantle suture and localization of deformation in

the weak Songpan-Ganzi complex rather than the stronger Tarim.

[65] 6. A model of continental deformation, which integrates key aspects of the microplate and continuum views, appears to provide the most accurate description of continental deformation within the Indo-Asian collision. Specifically, the continental mantle lithosphere appears to be broken into microplates along lithospheric scale structures such as the Altyn Tagh fault [Tapponnier *et al.*, 2001; Wittlinger *et al.*, 1998]. However, the extent to which upper crustal deformation reflects the motion of these underlying blocks is a function of the strength of the middle to lower crust. In some regions, such as Tarim, the middle to lower crust is strong enough to maintain coupling between the brittle upper crust and the underlying block of mantle lithosphere; whereas elsewhere, such as within the Songpan-Ganzi complex in western Tibet, the upper crust has decoupled from the mantle lithosphere [Clark and Royden, 2000; Royden, 1996; Shen *et al.*, 2001], allowing the weak middle to lower crust to evacuate from this area to thicken the crust of central Tibet. The mechanical behavior of continental crust thus appears to be a strong function of its geologic evolution.

[66] **Acknowledgments.** Eric Cowgill thanks Chris Coath and Kevin McKeegan for their instruction in the use of the CAMECA ims 1270 ion microprobe and their assistance during zircon analyses and subsequent data reduction. We thank Cindy Ebinger, George Gehrels, and Carole Petit-Mariani for their reviews. Earlier versions of the manuscript were significantly improved by reviews from Cindy Ebinger, Todd Ehlers, Laurent Jolivet, Paul Kapp, Nadine McQuarrie, Mike Murphy, Edward Sobel, and Alex Webb. Discussions with Alex Robinson, Yuan Chao, Kari Cooper, Mike Taylor, and Jorge Vazquez also significantly improved the clarity of the ideas presented here. We thank Laura Veirs, Jamie Buscher, and Elizabeth Catlos for field assistance. Fieldwork was made possible by collaborators Chen Zhengle, Zhang Qing, and Zhang Shuanghong, and drivers from the Tarim Petroleum Corporation. Cumulative probability plots in Figure 2 were generated using Isoplot/Ex v 2.3 provided by Kenneth Ludwig. This project was supported by NSF grants EAR9614664 and EAR9725599. We acknowledge facility support from the Instrumentation and Facilities Program of the National Science Foundation.

References

- Allmendinger, R. W., and T. Gubbels, Pure and simple shear plateau uplift, Altiplano-Puna, Argentina and Bolivia, *Tectonophysics*, 259, 1–13, 1996.
- Arnaud, N. O., Apports de la thermochronologie 40Ar/39Ar sur feldspath potassique a la connaissance de la tectonique Cenozoique d'Asie, Ph.D. thesis, Univ. Blaise Pascal, Clermont-Ferrand, France, 1992.
- Arnaud, N. O., P. Vidal, P. Tapponnier, P. Matte, and W. M. Deng, The high K₂O volcanism of northwestern Tibet: Geochemistry and tectonic implications, *Earth Planet. Sci. Lett.*, 111, 351–367, 1992.
- Arrowsmith, J. R., and M. R. Strecker, Seismotectonic range-front segmentation and mountain-belt growth in the Pamir-Alai region, Kyrgyzstan (India-Eurasia collision zone), *Geol. Soc. Am. Bull.*, 111, 1665–1683, 1999.
- Avouac, J. P., and G. Peltzer, Active tectonics in southern Xinjiang, China: Analysis of terrace riser and normal fault scarp degradation along the Hotan-Qira fault system, *J. Geophys. Res.*, 98(B12), 21,773–21,807, 1993.
- Besse, J., and V. Courtillot, Revised and synthetic apparent polar wander paths of the African, Eurasian, North American and Indian plates, and true polar wander since 200 Ma, *J. Geophys. Res.*, 96, 4029–4050, 1991.
- Bird, P., Lateral extrusion of lower crust from under high topography in the isostatic limit, *J. Geophys. Res.*, 96, 10,275–10,286, 1991.
- Boulin, J., Hercynian and Eocimmerian events in Afghanistan and adjoining regions, *Tectonophysics*, 148, 253–278, 1988.
- Brace, W. F., and D. L. Kohlstedt, Limits on lithospheric stress imposed by laboratory experiments, *J. Geophys. Res.*, 85, 6248–6252, 1980.
- Burchfiel, B. C., and L. H. Royden, Tectonics of Asia 50 years after the death of Emile Argand, *Eclogae Geol. Helv.*, 84, 599–629, 1991.
- Burchfiel, B. C., Q. Deng, P. Molnar, L. Royden, Y. Wang, P. Zhang, and W. Zhang, Intracrustal detachment zones of continental deformation, *Geology*, 17(8), 448–452, 1989.
- Burtman, V. S., and P. Molnar, Geological and geophysical evidence for deep subduction of continental crust beneath the Pamir, *Spec. Publ. Geol. Soc. Am.*, 281, 76 pp., 1993.
- Carter, N., and M. C. Tsenn, Flow properties of continental lithosphere, *Tectonophysics*, 136, 27–63, 1987.
- Chen, Y., J. Cogné, and V. Courtillot, New Cretaceous paleomagnetic poles from Tarim Basin, northwestern China, *Earth Planet. Sci. Lett.*, 114, 17–38, 1992.
- Chen, Y., J.-P. Cogné, V. Courtillot, P. Tapponnier, and X. Y. Zhu, Cretaceous paleomagnetic results from western Tibet and tectonic implications, *J. Geophys. Res.*, 98, 17,981–17,999, 1993.
- Chen, Y., S. Gilder, N. Halim, J. P. Cogné, and V. Courtillot, New paleomagnetic constraints on central Asian kinematics: Displacement along the Altyn Tagh fault and rotation of the Qaidam Basin, *Tectonics*, 21(5), 1042, 10.1029/2001TC901030, 2002.
- Chinese State Bureau of Seismology, *The Altyn Tagh Active Fault System* (in Chinese with English abstract), 319 pp., Seismology, Beijing, 1992.
- Clark, M. K., and L. H. Royden, Topographic ooze; building the eastern margin of Tibet by lower crustal flow, *Geology*, 28(8), 703–706, 2000.
- Compston, W., I. S. Williams, and C. Meyer, U-Pb geochronology of zircons from Lunar Breccia 73217 using a sensitive, high mass resolution ion microprobe, *J. Geophys. Res.*, 89, 8525–8534, 1984.
- Coward, M. P., W. S. F. Kidd, Y. Pan, R. M. Shackleton, and H. Zhang, The structure of the 1985 Tibet Geotraverse, Lhasa to Golmud, *Philos. Trans. R. Soc. London, Ser. A*, 327, 307–336, 1988.
- Cowgill, E., Tectonic evolution of the Altyn Tagh-Western Kunlun fault system, northwestern China, Ph.D. thesis, Univ. of Calif., Los Angeles, 2001.
- Cowgill, E., A. Yin, P. Rumelhart, X. F. Wang, and Q. Zhang, Kinematics of the central Altyn Tagh fault system, NW China, *Eos Trans. AGU*, 78(46), Fall Meet. Suppl., F173, 1997.
- Cowgill, E., A. Yin, X. F. Wang, and Q. Zhang, Is the North Altyn fault part of a strike-slip duplex along the Altyn Tagh fault system?, *Geology*, 28(3), 255–258, 2000.
- Cowgill, E., A. Yin, T. M. Harrison, M. Grove, and X.-F. Wang, Oligocene initiation of the central Altyn Tagh fault system inferred from 40Ar/39Ar K-feldspar thermochronology, *Eos Trans. AGU*, 82(47), Fall Meet. Suppl., F1125–F1126, 2001.
- Delville, N., N. Arnaud, J.-M. Montel, F. Roger, M. Brunel, P. Tapponnier, and E. Sobel, Paleozoic to Cenozoic deformation along the Altyn Tagh fault in the Altun Shan massif area, eastern Qilian Shan, northeastern Tibet, China, in *Paleozoic and Mesozoic Tectonic Evolution of Central and Eastern Asia: From Continental Assembly to Intracontinental Deformation*, edited by M. S. Hendrix and G. A. Davis, *Geol. Soc. of Am. Mem.*, 194, 269–292, 2001.
- Deng, W., A preliminary study on the petrology and petrochemistry of the Quaternary volcanic rocks of northern Tibet autonomous region (in Chinese), *Acta Geol. Sin.*, 52, 148–162, 1978.
- Deng, W., Ophiolites, in *Geological Evolution of the Karakorum and Kunlun Mountains*, edited by Y. Pan, pp. 51–93, Seismology, Beijing, 1996.
- Dewey, J. F., and A. M. C. Sengör, Aegean and surrounding regions: Complex multiplate and continuum tectonics in a convergent zone, *Geol. Soc. Am. Bull.*, 90, 84–92, 1979.
- Dewey, J. F., R. M. Shackleton, C. Chang, and Y. Sun, The tectonic evolution of the Tibetan Plateau, *Philos. Trans. R. Soc. London, Ser. A*, 327, 379–413, 1988.
- England, P., and G. Houseman, Role of lithospheric strength heterogeneities in the tectonics of Tibet and neighboring regions, *Nature*, 315, 297–301, 1985.
- England, P., and G. Houseman, The mechanics of the Tibetan Plateau, *Philos. Trans. R. Soc. London, Ser. A*, 326, 301–320, 1988.
- England, P., and D. P. McKenzie, A thin viscous sheet model for continental deformation, *Geophys. J. R. Astron. Soc.*, 70, 295–321, 1982.
- Gaetani, M., G. Gosso, and U. Pognante, A geological transect from Kun Lun to Karakorum (Sinkiang, China): The western termination of the Tibetan Plateau. Preliminary note, *Terra Nova*, 2, 23–30, 1990.
- Gao, R., D. Li, D. Lu, Y. Li, D. Huang, R. Feng, G. Qian, and C. Tang, Deep seismic reflection profile across contact zone of West Kunlun and Tarim along the Xinjiang geotranssect in NW China, in *14th Annual Himalaya-Karakorum-Tibet Workshop*, edited by E. Sobel *et al.*, pp. 49–50, Kloster Ettal, Germany, 1999.
- Gao, R., D. Huang, D. Lu, G. Qian, Y. Li, C. Kuang, Q. Li, P. Li, R. Feng, and Y. Guan, Deep seismic reflection profile across the juncture zone between the Tarim Basin and the West Kunlun mountains, *Chin. Sci. Bull.*, 45(24), 2281–2286, 2000.

- Gehrels, G., A. Yin, X. Chen, and X. Wang, Preliminary U-Pb geochronologic studies along the Altyn Tagh fault, western China, *Eos Trans. AGU*, 80(46), Fall Meet. Suppl., F1018, 1999.
- Gilder, S., X. Zhao, R. Coe, Z. Meng, V. Courtillot, and J. Besse, Paleomagnetism and tectonics of the southern Tarim basin, northwestern China, *J. Geophys. Res.*, 101, 22,015–22,031, 1996.
- Girardeau, J., J. Marcoux, and C. Montenat, The neo-Cimmerian ophiolite belt in Afghanistan and Tibet: Comparison and evolution, in *Tectonic Evolution of the Tethyan Region*, edited by A. M. C. Sengör, pp. 477–504, Kluwer Acad., Norwell, Mass., 1989.
- Grier, M. E., J. A. Salfity, and R. W. Allmendinger, Andean reactivation of the Cretaceous Salta rift, northwestern Argentina, *J. S. Am. Earth Sci.*, 4(4), 351–372, 1991.
- Hacker, B. R., X. Wang, E. A. Eide, and L. Ratschbacher, The Qinling-Dabie ultra-high-pressure collisional orogen, in *The Tectonic Evolution of Asia*, edited by A. Yin and T. M. Harrison, pp. 345–370, Cambridge Univ. Press, New York, 1996.
- Hacker, B. R., E. Gnos, L. Ratschbacher, M. Grove, M. McWilliams, S. V. Sobolev, J. Wan, and Z. Wu, Hot and dry deep crustal xenoliths from Tibet, *Science*, 287, 2463–2466, 2000a.
- Hacker, B. R., L. Ratschbacher, L. Webb, M. O. McWilliams, T. Ireland, A. Calvert, S. Dong, H.-R. Wenk, and D. Chateigner, Exhumation of ultrahigh-pressure continental crust in east central China: Late-Triassic-Early Jurassic tectonic unroofing, *J. Geophys. Res.*, 105, 13,339–13,364, 2000b.
- Hamburger, M. W., D. R. Sarewitz, T. L. Pavlis, and G. A. Popandopulo, Structural and seismic evidence for intracontinental subduction in the Peter the First Range, Central Asia, *Geol. Soc. Am. Bull.*, 104, 397–408, 1992.
- Hanson, A., Evidence of Cenozoic erosional unroofing adjacent to the northern Qaidam basin, NW China, preserved within basin margin strata, *Geol. Soc. Am. Abstr. Programs*, 29, A-143, 1997.
- Haq, B., and F. W. B. Van Eysinga, *Geologic Time Table*, Elsevier Sci., New York, 1998.
- Harris, N. B. W., R. Xu, C. L. Lewis, C. J. Hawkesworth, and Y. Zhang, Isotope geochemistry of the 1985 Tibet Geotraverse, Lhasa to Golmud, *Philos. Trans. R. Soc. London, Ser. A*, 327, 263–285, 1988.
- Houseman, G. A., and P. England, A lithospheric-thickening model for the Indo-Asian collision, in *The Tectonic Evolution of Asia*, edited by A. Yin and T. M. Harrison, pp. 3–17, Cambridge Univ. Press, New York, 1996.
- Hsü, K. J., Relict back-arc basins: Principles of recognition and possible new examples from China, in *New Perspectives in Basin Analysis*, edited by K. L. Kleinsphen and C. Paola, pp. 245–263, Springer-Verlag, New York, 1988.
- Hsü, K. J., et al., Tectonic evolution of the Tibetan Plateau: A working hypothesis based on the archipelago model of orogenesis, *Int. Geol. Rev.*, 37, 473–508, 1995.
- Isacks, B., J. Oliver, and L. R. Sykes, Seismology and the new global tectonics, *J. Geophys. Res.*, 73, 5855–5899, 1968.
- Jia, C., *Tectonic Characteristics and Petroleum, Tarim Basin, China*, 295 pp., Pet. Ind. Press, Beijing, 1997.
- Jiang, C., J. Yang, B. Feng, Z. Zhu, M. Zhao, Y. Chai, X. Shi, H. Wang, and J. Hu, *Opening-Closing Tectonics of Kunlun Mountains* (in Chinese), 224 pp., Geol. Publ. House, Beijing, 1992.
- Jordan, T. E., and M. Gardeweg, Tectonic evolution of the late Cenozoic central Andes (20°–33°S), in *The Evolution of the Pacific Ocean Margins*, edited by Z. Ben-Avraham, pp. 193–207, Oxford Univ. Press, New York, 1989.
- Jordan, T. E., B. L. Isacks, R. W. Allmendinger, J. A. Brewer, V. A. Ramos, and C. J. Ando, Andean tectonics related to geometry of subducted Nazca plate, *Geol. Soc. Am. Bull.*, 94, 341–361, 1983.
- Kao, H., R. Gao, R.-J. Rau, Y. Guan, R.-Y. Chen, and D. Shi, Seismological evidence against the subduction of Tarim block beneath Tibet: Preliminary results from a broadband seismic experiment along the Tarim-Tibet border, *Eos Trans. AGU*, 80(46), Fall Meet. Suppl., F1008, 1999.
- Kao, H., R. Gao, R.-J. Rau, D. Shi, R.-Y. Chen, Y. Guan, and F. T. Wu, Seismic image of the Tarim basin and its collision with Tibet, *Geology*, 29(7), 575–578, 2001.
- Kapp, P., A. Yin, C. E. Manning, M. Murphy, T. M. Harrison, M. Spurlin, D. Lin, D. X1-Guang, and W. Cun-Ming, Blueschist-bearing metamorphic core complexes in the Qiangtang block reveal deep crustal structure of northern Tibet, *Geology*, 28(1), 19–22, 2000.
- Kidd, W. S. F., and P. Molnar, Quaternary and active faulting observed on the 1985 Academia Sinica-Royal Society geotraverse of Tibet, *Philos. Trans. R. Soc. London, Ser. A*, 327, 337–363, 1988.
- Kidd, W. S. F., Y. Pan, C. Chang, M. P. Coward, J. F. Dewey, A. Gansser, P. Molnar, R. M. Shackleton, and Y. Sun, Geological mapping of the 1985 Chinese-British Tibetan (Xizang-Qinghai) Plateau geotraverse route, *Philos. Trans. R. Soc. London, Ser. A*, 327, 287–305, 1988.
- Kong, X., and P. Bird, Neotectonics of Asia: Thin-shell finite-element models with faults, in *The Tectonic Evolution of Asia*, edited by A. Yin and T. M. Harrison, pp. 18–34, Cambridge Univ. Press, New York, 1996.
- Lamb, M. A., A. D. Hanson, S. A. Graham, G. Badarch, and L. E. Webb, Left-lateral sense offset of upper Proterozoic to Paleozoic features across the Gobi Onon, Tost, and Zuunbayan faults in southern Mongolia and implications for other central Asian faults, *Earth Planet. Sci. Lett.*, 173, 183–194, 1999.
- Laveine, J.-P., Z. Shanzhen, Y. Lemoigne, A. Desheng, Z. Qishi, and C. Jingyuan, The Upper Paleozoic floras of Hotan area (Xinjiang Province, northwest China), and their paleogeographical significance, *C. R. Acad. Sci., Ser. II*, 322(9), 781–790, 1996.
- Leeder, M. R., A. B. Smith, and J. Yin, Sedimentology, paleoecology and palaeoenvironmental evolution of the 1985 Lhasa to Golmud Geotraverse, *Philos. Trans. R. Soc. London, Ser. A*, 327, 107–143, 1988.
- Li, D., D. Liang, C. Jia, G. Wang, Q. Wu, and D. He, Hydrocarbon accumulations in the Tarim basin, China, *AAPG Bull.*, 80(10), 1587–1603, 1996.
- Liu, Z. Q., *Geologic Map of the Qinghai-Xizang Plateau and its Neighboring Regions* (in Chinese), Chengdu Inst. of Geol. and Miner. Resour., Acad. Sin. Geol. Publ., Beijing, 1988.
- Lyon-Caen, H., and P. Molnar, Gravity anomalies and the structure of western Tibet and the southern Tarim basin, *Geophys. Res. Lett.*, 11(12), 1251–1254, 1984.
- Ma, X., *Lithospheric Dynamics Map of China and Adjacent Seas*, Geol. Publ. House, Beijing, 1980.
- Mattauer, M., Intracontinental subduction, crust-mantle décollement and crustal-stacking wedge in the Himalayas and other collisional belts, in *Collision Tectonics*, edited by M. P. Coward and A. C. Ries, pp. 37–50, Geol. Soc. Spec. Publ., London, 1986.
- Matte, P., P. Tapponnier, N. Arnaud, L. Bourjot, J. P. Avouac, P. Vidal, Q. Liu, Y. Pan, and Y. Wang, Tectonics of western Tibet, between the Tarim and the Indus, *Earth Planet. Sci. Lett.*, 142, 311–330, 1996.
- Mattern, F., W. Schneider, Y. Li, and X. Li, A traverse through the western Kunlun (Xinjiang, China): Tentative geodynamic implications for the Paleozoic and Mesozoic, *Geol. Rundsch.*, 85, 705–722, 1996.
- McKenzie, D., Active tectonics of the Mediterranean region, *Geophys. J. R. Astron. Soc.*, 30, 109–185, 1972.
- McKenzie, D. P., Plate tectonics of the Mediterranean region, *Nature*, 226, 239–243, 1970.
- McQuarrie, N., and C. G. Chase, Raising the Colorado Plateau, *Geology*, 28(1), 91–94, 2000.
- McQuarrie, N., and P. G. DeCelles, Geometry and structural evolution of the central Andean backthrust belt, Bolivia, *Tectonics*, 20(5), 669–692, 2001.
- Meyer, B., P. Tapponnier, L. Bourjot, F. Metivier, Y. Gaudemer, G. Peltzer, S. Guo, and Z. Chen, Crustal thickening in Gansu-Qinghai, lithospheric mantle subduction, and oblique, strike-slip controlled growth of the Tibet plateau, *Geophys. J. Int.*, 135, 1–47, 1998.
- Molnar, P., Brace-Goetze strength profiles, the partitioning of strike-slip and thrust faulting at zones of oblique convergence, and the stress-heat flow paradox of the San Andreas fault, in *Fault Mechanics and Transport Properties of Rocks*, edited by B. Evans and T. F. Wong, pp. 435–459, Academic, San Diego, Calif., 1992.
- Molnar, P., and P. Tapponnier, Active tectonics of Tibet, *J. Geophys. Res.*, 83, 5361–5375, 1978.
- Molnar, P., and P. Tapponnier, Cenozoic tectonics of Asia; effects of a continental collision, *Science*, 189, 419–426, 1975.
- Molnar, P., and P. Tapponnier, A possible dependence of tectonic strength on the age of the crust in Asia, *Earth Planet. Sci. Lett.*, 52, 107–114, 1981.
- Molnar, P., B. C. Burchfiel, L. K'uangyi, and Z. Ziyun, Geomorphic evidence for active faulting in the Altyn Tagh and northern Tibet and qualitative estimates of its contribution to the convergence of India and Eurasia, *Geology*, 15(3), 249–253, 1987a.
- Molnar, P., B. C. Burchfiel, Z. Zhao, K. Liang, S. Wang, and M. Huang, Geologic evolution of northern Tibet: Results of an expedition to Ulugh Muztagh, *Science*, 235, 299–305, 1987b.
- Murphy, M. A., A. Yin, T. M. Harrison, S. B. Dürr, Z. Chen, F. J. Ryerson, W. S. F. Kidd, X. Wang, and X. Zhou, Did the Indo-Asian collision alone create the Tibetan Plateau?, *Geology*, 25(8), 719–722, 1997.
- Murphy, M. A., A. Yin, P. Kapp, T. M. Harrison, L. Din, and J. Guo, Southward propagation of the Karakorum fault system into southwest Tibet: Timing and magnitude of slip, *Geology*, 28(5), 451–454, 2000.
- Neil, E. A., and G. A. Houseman, Geodynamics of the Tarim Basin and the Tian Shan in central Asia, *Tectonics*, 16(4), 571–584, 1997.
- Nelson, K. D., et al., Partially molten middle crust beneath southern Tibet: Synthesis of project INDEPTH results, *Science*, 274, 1684–1688, 1996.
- Nie, S., Paleoclimatic and paleomagnetic constraints on the Paleozoic reconstructions of South China, North China and Tarim, *Tectonophysics*, 196, 279–308, 1991.

- Norin, E., *Geological Explorations in Western Tibet, Reports From the Scientific Expedition to the North-Western Provinces of China Under the Leadership of Dr. Sven Hedin, Publ. 29, III Geology*, 214 pp., Tryckeri Aktiebolaget Thule, Stockholm, Sweden, 1946.
- Owens, T. J., and G. Zandt, Implications of crustal property variations for models of Tibetan Plateau evolution, *Nature*, 387, 37–43, 1997.
- Paces, J. B., and J. D. Miller, Precise U-Pb age of Duluth Complex and related mafic intrusions, northeastern Minnesota: Geochronological insights into physical, petrogenic, paleomagnetic and tectonomagmatic processes associated with the 1.1 Ga midcontinent rift system, *J. Geophys. Res.*, 98, 13,997–14,013, 1993.
- Pan, G. T., Cenozoic structures and the nature of mountain building in the Altyn Tagh region (in Chinese), *Geol. Qinghai-Xizang Tibet Plateau*, 15, 113–120, 1984.
- Pan, Y., Tectonic features and evolution of the Western Kunlun Mountain region, *Sci. Geol. Sin.*, 1990(3), 224–232, 1990.
- Pan, Y., *Geological Evolution of the Karakorum and Kunlun Mountains*, 288 pp., Seismology, Beijing, 1996a.
- Pan, Y. S., Regional geological evolution and conclusion, in *Geological Evolution of the Karakorum and Kunlun Mountains*, edited by Y. S. Pan, pp. 263–282, Seismology, Beijing, 1996b.
- Peltzer, G., and P. Tapponnier, Formation and evolution of strike-slip faults, rifts, and basins during the India-Asia collision: An experimental approach, *J. Geophys. Res.*, 93, 15,085–15,117, 1988.
- Peltzer, G., P. Tapponnier, and R. Armijo, Magnitude of late Quaternary left-lateral movement along the north edge of Tibet, *Science*, 246, 1285–1289, 1989.
- Quidelleur, X., M. Grove, O. M. Lovera, T. M. Harrison, and A. Yin, Thermal evolution and slip history of the Rembu Zedong thrust, south-eastern Tibet, *J. Geophys. Res.*, 102, 2659–2679, 1997.
- Ranalli, G., and D. C. Murphy, Rheological stratification of the lithosphere, *Tectonophysics*, 132, 281–295, 1987.
- Ritts, B. D., and U. Biffi, Magnitude of post-Middle Jurassic (Bajocian) displacement on the Altyn Tagh fault system, Northwest China, *Geol. Soc. Am. Bull.*, 112, 61–74, 2000.
- Roeder, D., Andean-age structure of eastern Cordillera (province of La Paz, Bolivia), *Tectonics*, 7(1), 23–39, 1988.
- Royden, L., Coupling and decoupling of crust and mantle in convergent orogens: Implications for strain partitioning in the crust, *J. Geophys. Res.*, 101, 17,679–17,705, 1996.
- Royden, L. H., B. C. Burchfiel, R. W. King, E. Wang, Z. Chen, F. Shen, and Y. Liu, Surface deformation and lower crustal flow in eastern Tibet, *Science*, 276, 788–790, 1997.
- Rumelhart, P., A. Yin, E. Cowgill, R. Butler, Q. Zhang, and X. F. Wang, Cenozoic vertical-axis rotation of the Altyn Tagh fault system, *Geology*, 27(9), 819–822, 1999.
- Rumelhart, P. E., Cenozoic basin evolution of southern Tarim, northwestern China: Implications for the uplift history of the Tibetan Plateau, Ph.D. thesis, Univ. of Calif., Los Angeles, 1998.
- Ryerson, F. J., G. Peltzer, P. Tapponnier, R. C. Finkel, A.-S. Meriaux, J. Van der Woerd, and M. W. Caffee, Active slip rates on the Altyn Tagh fault Karakax valley segment: Constraints from surface exposure age dating, *Eos Trans. AGU*, 80(46), Fall Meet. Suppl., F1008, 1999.
- Sañudo-Wilhelmy, S. A., and A. R. Flegal, Temporal variations in lead concentrations and isotopic composition in the southern California Bight, *Geochim. Cosmochim. Acta*, 58(15), 3315–3320, 1994.
- Searle, M. P., Geological evidence against large-scale pre-Holocene offsets along the Karakoram fault: Implications for the limited extrusion of the Tibetan Plateau, *Tectonics*, 15(1), 171–186, 1996.
- Sengör, A. M. C., *The Cimmeride Orogenic System and the Tectonics of Eurasia, Spec. Pap. 195*, 82 pp., Geol. Soc. of Am., Boulder, Colo., 1984.
- Sengör, A. M. C., The Palaeo-Tethyan suture: A line of demarcation between two fundamentally different architectural styles in the structure of Asia, *Island Arc*, 1, 78–91, 1992.
- Sengör, A. M. C., and B. A. Natal'in, Paleotectonics of Asia: Fragments of a synthesis, in *The Tectonic Evolution of Asia*, edited by A. Yin and T. M. Harrison, pp. 486–640, Cambridge Univ. Press, New York, 1996.
- Sengör, A. M. C., and A. H. Okurogullari, The role of accretionary wedges in the growth of continents: Asiatic examples from Argand to plate tectonics, *Eclogae Geol. Helv.*, 84, 535–597, 1991.
- Sengör, A. M. C., S. A. Graham, and K. T. Biddle, Is the Tarim basin underlain by a Neoproterozoic ocean plateau?, *Geol. Soc. Am. Abstr. Programs*, 28, 67, 1996.
- Shen, F., L. H. Royden, and B. C. Burchfiel, Large-scale crustal deformation of the Tibetan Plateau, *J. Geophys. Res.*, 106, 6793–6816, 2001.
- Shen, Z.-K., M. Wang, Y. Li, D. D. Jackson, A. Yin, D. Dong, and P. Fang, Crustal deformation along the Altyn Tagh fault system, western China, from GPS, *J. Geophys. Res.*, 106, 30,607–30,621, 2001.
- Sobel, E. R., Basin analysis and apatite fission-track thermochronology of the Jurassic-Paleogene southwest Tarim basin, NW China, Ph.D. thesis, Stanford Univ. Press, Stanford, Calif., 1995.
- Sobel, E. R., and N. Arnaud, A possible middle Paleozoic suture in the Altyn Tagh, NW China, *Tectonics*, 18(1), 64–74, 1999.
- Sobel, E. R., N. Arnaud, M. Jolivet, B. D. Ritts, and M. Brunel, Jurassic to Cenozoic exhumation history of the Altyn Tagh range, Northwest China, constrained by ⁴⁰Ar/³⁹Ar and apatite fission track thermochronology, in *Paleozoic and Mesozoic Tectonic Evolution of Central and Eastern Asia: From Continental Assembly to Intracontinental Deformation*, edited by M. S. Hendrix and G. A. Davis, *Geol. Soc. of Am. Mem.*, 194, pp. 247–267, Geol. Soc. of Am., Boulder, Colo., 2001.
- Soofi, M. A., and S. D. King, Oblique convergence between India and Eurasia, *J. Geophys. Res.*, 107(B5), 2101, doi:10.1029/2001JB000636, 2002.
- Stacey, J. S., and J. D. Kramers, Approximation of terrestrial lead isotope evolution by a two-stage model, *Earth Planet. Sci. Lett.*, 26, 207–221, 1975.
- Stöcklin, J., Tethys evolution in the Afghanistan-Pamir-Pakistan region, in *Tectonic Evolution of the Tethyan Region*, edited by A. M. C. Sengör, pp. 241–264, Kluwer Acad., Norwell, Mass., 1989.
- Strecker, M. R., W. Frisch, M. W. Hamburger, L. Ratschbacher, S. Semilekin, A. Zamoruyev, and N. Sturchio, Quaternary deformation in the eastern Pamir, Tadzhikistan, and Kyrgyzstan, *Tectonics*, 14, 1061–1079, 1995.
- Tapponnier, P., and P. Molnar, Slip-line field theory and large-scale continental tectonics, *Nature*, 264, 319–324, 1976.
- Tapponnier, P., and P. Molnar, Active faulting and tectonics in China, *J. Geophys. Res.*, 82, 2905–2930, 1977.
- Tapponnier, P., G. Peltzer, A. Y. Le Dain, and R. Armijo, Propagating extrusion tectonics in Asia: New insights from simple experiments with plasticine, *Geology*, 10(12), 611–616, 1982.
- Tapponnier, P., et al., Active thrusting and folding in the Qilian Shan and decoupling between upper crust and mantle in northeastern Tibet, *Earth Planet. Sci. Lett.*, 97, 382–403, 1990.
- Tapponnier, P., Z. Xu, F. Roger, B. Meyer, N. Arnaud, G. Wittlinger, and J. Yang, Oblique stepwise rise and growth of the Tibet Plateau, *Science*, 294, 1671–1677, 2001.
- Turcotte, D. L., and G. Schubert, *Geodynamics*, 450 pp., John Wiley, New York, 1982.
- Van der Woerd, J., F. J. Ryerson, P. Tapponnier, Y. Gaudemer, R. Finkel, A. S. Meriaux, M. Caffee, G. Zhao, and Q. He, Holocene left-slip rate determined by cosmogenic surface dating on the Xidatan segment of the Kunlun fault (Qinghai China), *Geology*, 26(8), 695–698, 1998.
- Van der Woerd, J., F. J. Ryerson, P. Tapponnier, A. S. Meriaux, Y. Gaudemer, B. Meyer, R. C. Finkel, M. W. Caffee, G. Zhao, and Z. Xu, Uniform slip-rate along the Kunlun fault: Implications for seismic behaviour and large-scale tectonics, *Geophys. Res. Lett.*, 27, 2353–2356, 2000.
- Vilotte, J. P., M. Daignières, and R. Madariaga, Numerical modeling of intraplate deformation: Simple mechanical models of continental collision, *J. Geophys. Res.*, 87, 10,709–10,728, 1982.
- Vilotte, J. P., M. Daignières, R. Madariaga, and O. C. Zienkiewicz, The role of a heterogeneous inclusion during continental collision, *Phys. Earth Planet. Inter.*, 36, 236–259, 1984.
- Washburn, Z., J. R. Arrowsmith, S. L. Forman, E. Cowgill, X. Wang, Y. Zhang, and Z. Chen, Late Holocene earthquake history of the central Altyn Tagh fault, China, *Geology*, 29(11), 1051–1054, 2001.
- Watson, M. P., A. B. Hayward, D. N. Parkinson, and Z. M. Zhang, Plate tectonic history, basin development and petroleum source rock deposition onshore China, *Mar. Pet. Geol.*, 4, 205–225, 1987.
- Wittlinger, G., P. Tapponnier, G. Poupinet, M. Jiang, D. Shi, G. Herquel, and F. Masson, Tomographic evidence for localized lithospheric shear along the Altyn Tagh fault, *Science*, 282, 74–76, 1998.
- Xiao, W. J., B. F. Windley, H. L. Chen, G. C. Zhang, and J. L. Li, Carboniferous-Triassic subduction and accretion in the western Kunlun, China: Implications for the collisional and accretionary tectonics of the northern Tibetan Plateau, *Geology*, 30(4), 295–298, 2002a.
- Xiao, W. J., B. F. Windley, J. Hao, and J. Li, Arc-ophiolite obduction in the Western Kunlun Range (China): Implications for the Palaeozoic evolution of Central Asia, *J. Geol. Soc. London*, 159, 517–528, 2002b.
- Xinjiang Bureau of Geology and Mineral Resources, *Regional Geology of Xinjiang Uygur Autonomous Region* (in Chinese with English abstract), 841 pp., Geol. Publ. House, Beijing, 1993.
- Xu, R., and N. B. W. Harris, Isotope geochemistry of the 1985 Tibet Geotraverse, Lhasa to Golmud (in Chinese), in *The Geological Evolution of Tibet*, pp. 282–302, Science Press, Beijing, 1990.
- Xu, R., Y. Zhang, Y. Xie, P. Vidal, N. Arnaud, Q. Zhang, and D. Zhao, Isotopic geochemistry of plutonic rocks, in *Geological Evolution of the Karakorum and Kunlun Mountains*, edited by Y. Pan, pp. 137–186, Seismol. Press, Beijing, 1996.

- Yao, Y., and K. J. Hsü, Origin of the Kunlun Mountains by arc-arc and arc-continent collisions, *Island Arc*, 3, 75–89, 1992.
- Yin, A., and T. M. Harrison, Geologic evolution of the Himalayan-Tibetan Orogen, *Annu. Rev. Earth Planet. Sci.*, 28, 211–280, 2000.
- Yin, A., and S. Nie, An indentation model for the North and South China collision and the development of the Tanlu and Honam fault systems, *Tectonics*, 12, 801–813, 1993.
- Yin, A., and S. Nie, A Phanerozoic palinspastic reconstruction of China and its neighboring regions, in *The Tectonic Evolution of Asia*, edited by A. Yin and T. M. Harrison, pp. 442–485, Cambridge Univ. Press, New York, 1996.
- Yin, A., S. Nie, P. Craig, T. M. Harrison, F. J. Ryerson, X. Qian, and G. Yang, Late Cenozoic tectonic evolution of the southern Chinese Tian Shan, *Tectonics*, 17(1), 1–27, 1998.
- Yin, A., Z. Yang, R. Butler, Y.-I. Otofujii, P.E. Rumelhart, and E. Cowgill, Correction: Cenozoic vertical-axis rotation of the Altyn Tagh fault system, *Geology*, 28, 480, 2000.
- Yin, A., et al., Tectonic history of the Altyn Tagh fault system in northern Tibet inferred from Cenozoic sedimentation, *Geol. Soc. Am. Bull.*, 114(5), 1257–1295, 2002.
- Yin, J., J. Xu, C. Liu, and H. Li, The Tibetan Plateau: Regional stratigraphic context and previous work, *Philos. Trans. R. Soc. London, Ser. A*, 327, 5–52, 1988.
- Yuan, C., M. Sun, M.-F. Zhou, H. Zhou, W.-J. Xiao, and J.-L. Li, Tectonic evolution of the West Kunlun: Geochronologic and geochemical constraints from Kudi granitoids, *Int. Geol. Rev.*, 44, 653–669, 2002.
- Zhang, H. M., J. G. Liou, and R. G. Coleman, An outline of the plate tectonics of China, *Geol. Soc. Am. Bull.*, 95, 295–312, 1984.
- Zhang, Z. T., Geologic characteristics of the Altyn Tagh (in Chinese), *Bull. Xian Inst. Geol. Chin. Acad. Geol. Sci.*, 9, 19–32, 1985.
- Zhou, H.-W., R. Gao, M. A. Murphy, Q. Li, and A.-R. Khalid, Deep seismic reflection profiling in northwest Tibetan Plateau: Implications for the relationship between the Tibetan Plateau, west Kunlun Shan, and Tarim Basin, *Eos Trans. AGU*, 81(48), Fall Meet. Suppl., F1091, 2000.
- Zhu, S. N., Tectonic evolution of the Qilian Shan, western China, *Bull. Changcun Geol. Coll.*, 3, 41–52, 1986.

E. Cowgill, Division of Geological and Planetary Sciences, California Institute of Technology, MC 100-23, Pasadena, CA 91125, USA. (ecowgill@gps.caltech.edu)

T. M. Harrison and A. Yin, Department of Earth and Space Sciences and Institute of Geophysics and Planetary Physics, University of California, Los Angeles, CA 90095-1567, USA.

X.-F. Wang, Institute of Geomechanics, Chinese Academy of Geological Sciences, Beijing 100081, China.